Am J Transl Res 2023;15(6):3942-3959
www.ajtr.org /ISSN:1943-8141/AJTR0145911

Original Article

A novel cuproptosis-related signature predicts prognosis and immunotherapy efficacy in lung adenocarcinoma

Yao Cui, Lu-Jin Zhang, Yu-Jie Xu, Ming-Yue Liu

Department of Oncology, Henan Provincial People's Hospital, People's Hospital of Zhengzhou University, Henan University People's Hospital, Zhengzhou 450003, Henan, China

Received August 13, 2022; Accepted March 28, 2023; Epub June 15, 2023; Published June 30, 2023

Abstract: Background: Lung adenocarcinoma (LUAD) is the leading histological subtype of lung cancer worldwide, causing high annual mortality. Tsvetkov et al. recently found a new form of regulated cell death, termed cuproptosis. The prognostic value of cuproptosis-related gene signature in LUAD remains uncertain. Methods: A training cohort is identified by the TCGA-LUAD dataset, whereas validation cohorts one and two are identified by GSE72094 and GSE68465, respectively. GeneCard and GSEA were used to extract genes related to cuproptosis. Cox regression, Kaplan-Meier regression, and LASSO regression were used to construct a gene signature. The model's applicability was evaluated by Kaplan-Meier estimators, Cox models, ROC, and tAUC across two independent validation cohorts. We examined the model's connections with other forms of regulated cell death. The immunotherapy ability of the signature was demonstrated by applying TMB, immune relevant signatures, and TIDE. The GSEA and immune infiltration analysis offer a better understanding of how the signature functions and the role of immune cells in its prognostic power. Results: A ten-gene signature was built and demonstrated owning prognostic power by being applied to the validation cohorts. The GSEA uncovered that the unfolded protein response, glycolysis/gluconeogenesis, and MYC were highly related to the gene signature. The ten-gene signature is closely related to related genes of apoptosis, necroptosis, pyroptosis, and ferroptosis. Our signature may have utility in predicting immunotherapy efficacy in LUADs. Mast cells were identified as key players that support the predicting capacity of the ten-gene signature through the immune infiltrating analysis. Conclusions: The novel ten-gene signature associated with apoptosis in cuproptosis that we obtained may contribute to improved LUAD management strategies and the ability to predict response to LUAD immunotherapy. It is suggested that mast cell infiltration might be related to the prognostic power of this signature.

Keywords: Lung adenocarcinoma, cuproptosis, copper, tumor microenvironment, gene signature

Introduction

Lung cancer is one of the most life-threatening diseases, with significantly high morbidity [1]. Most lung cancer cases are adenocarcinoma (LUAD), a histological subtype that accounts for 40% of all lung cancer cases [1]. Commonly known prognostic factors of LUAD include TNM stage, degree of tumor differentiation, and pathological subtype [2]. Clinical decision-making is still dominated by these factors, but 5-year survival rates for lung cancer patients are still low, ranging from 4%-17% [2]. For the current research on LUAD, finding new, specific, and effective prognostic biomarkers or establishing a corresponding prognostic signature is very important.

Regulated cell death, which plays a key role in organismal development, homeostasis, and pathogenesis, is inextricably linked to cancer and has been widely reported [3]. Cancer cells often respond to their altered state during tumor progression by programmed cell death [3]. It has been demonstrated in long-term studies that regulated cell death aids in cancer treatment, but it is a double-edged sword since normal cells also die as a result [3]. It is important to note that LUAD's therapeutic response is influenced by several regulated cell death mechanisms [4-8], including apoptosis, necroptosis, pyroptosis, and ferroptosis. Excitingly, Tsvetkov and colleagues published their latest study in the journal *Science*, confirming the existence of copper-induced regulated cell de-

ath, which is termed cuproptosis [9]. In their study, it was shown that cuproptosis is distinct from apoptosis, necroptosis, pyroptosis, and ferroptosis [9]. Given that some forms of regulated cell death may be more immunologically targeted than others, learning how cuproptosis is initiated, propagated, and ultimately performed may have important implications for possible combination diagnosis and therapeutic intervention [10].

Many researchers have developed prognostic models for LUAD and demonstrated that they are more stable and applicable than a single prognostic biomarker [7, 8, 11-16]. There is, however, little understanding of the relationship between "new" cuproptosis and the progression mechanism and prognosis of LUAD, and cuproptosis has not been used to construct a LUAD prognosis model. To fill this gap, our study aimed to identify a prognostic signature for LUAD by integrating multiple datasets. We gathered cuproptosis-related genes constructing a gene signature having the ability to predict LUAD outcomes, and further validated its prognostic ability in other independent datasets. We also tested the model's connections with other types of regulated cell death. More importantly, the immunotherapy potential of the model was examined. An analysis of gene set enrichment analysis (GSEA) and tumor-infiltrating immune cells was carried out at the end of the study.

Materials and methods

Public database selection

The TCGA-LUAD project contains sequencing and clinical data from LUAD samples. We obtained TCGA-LUAD dataset from GDC Xena Hub (https://gdc.xenahubs.net) [17]. To obtain more LUAD samples, we searched the Gene Expression Omnibus (GEO) database [18] (https://www.ncbi.nlm.nih.gov/geo/) using the keyword "lung adenocarcinoma" and selected the dataset whose total RNA expression and survival data is available, and eliminated the datasets with total case numbers less than 390. In the end, two candidate datasets appeared, namely GSE72094 and GSE68465. As part of the preprocessing, we removed samples without gene expression data or samples without survival data from the datasets that we selected above. This study uses TCGA-LUAD as the training cohort, and GSE72094 and GSE68465 as the validation cohorts.

Screening of cuproptosis-related genes

We screened cuproptosis-related genes according to the following criteria: 1) We searched GeneCard (https://www.genecards.org/) using the keyword "copper"; 2) We searched the GSEA (https://www.gsea-msigdb.org/gsea/msigdb/search.jsp) website using the keyword "copper"; 3) We took the unique genes from the union of the results obtained above as the cuproptosis-related genes.

Construction and validation of the prognosis model

A Cox regression model and Kaplan-Meier analysis were performed in the R language environment using the "survival" and "survminer" R packages to screen cuproptosis-related genes with prognostic ability. We applied the LASSO analysis performed by the 'glmnet' R package to minimize the overfitting of the aforementioned prognostic genes [19-22]. The running parameter was set to be 10-fold cross-validation. A reduced dimensionality coefficient is calculated for each gene by LASSO, which is used to calculate each patient's risk score (βi denotes the coefficient, Expi represents the relative expression level, and n indicates each hub gene):

$$Risk\ score = \sum_{i}^{n} Expi * \beta i$$

We use the median to stratify and divide patients into high- and low-risk groups in the partial validation process. We performed separate validation analyses in all the studied cohorts, including Kaplan-Meier analysis, univariate Cox analysis, multivariate Cox analysis, ROC analysis, and tAUC analysis [23]. We completed the above analyses in the R language environment with the "timeROC" and "survival" packages.

Gene set enrichment analysis (GSEA)

Hallmarked biological differences between high-risk and low-risk groups were examined using GSEA using hallmark gene sets [24, 25]. The analysis was performed using GSEA software, and *p*-values and FDRs were considered

statistically significant at 0.05 and 0.25, respectively.

Correlations between the gene signature and apoptosis, necroptosis, pyroptosis, and ferroptosis

To better know the interactions between gene signature and other forms of regulated cell death, we adopted a comprehensive analysis that consisted of the Pearson analysis and Wilcoxon rank-sum. Apoptosis, necroptosis, and pyroptosis-related genes were extracted from the GeneCard and GSEA online databases, respectively, by applying the following steps: 1) searching the GeneCard using the Corresponding keyword; 2) searching the GSEA using the Corresponding keyword: 3) merging the above results and taking the unique genes. In addition, ferroptosis-related genes were obtained from the FerrDb online portal (http://www.datjar.com:40013/bt2104/) [26].

Correlations between the gene signature and immunotherapy

TMB - tumor mutational burden - measures the immune response by quantifying how frequently specific mutations occur within tumor genes [27]. Our method of calculating the TMB score for each patient with LUAD was based on previously published studies [27]. For the correlation between risk score and TMB, we used the Pearson coefficient and Wilcoxon rank-sum. Then, we selected CD274 [28], CTLA4 [29], HAVCR2 [30], IDO1 [31], LAG3 [32], PDCD1 [33], CD8A [34], CXCL10 [35], CXCL9 [36], GZMA [37], GZMB [38], IFNG [39], PRF1 [40], TBX2 [41], and TNF [42] from previous studies as immune relevant signatures. Pearson and Wilcoxon rank-sum analysis measured the correlation between our signature and these immune-relevant signatures. To judge whether our gene signature has the potential ability to guide immunotherapy, we created a Kaplan-Meier analysis to test the prognostic sensitivity of individual immune-related signatures in high-risk and low-risk patients, respectively. The new and widely cited Tumor Immune Dysfunction and Exclusion (TIDE) computational framework is capable of modeling tumor immune evasion using dysfunctional expression signatures of T cells and T cell exclusion, providing predictability for immunotherapy treatments [43-45]. As part of this study, we applied the TIDE score to examine whether our signatures were correlated.

Relationships between the TICs and our signature

TICs play a crucial role in the initiation and progression of cancer [46]. Using expression data from the training cohort, we estimated the abundance of 22 TICs expressed in LUAD. Afterward, we first used Pearson and Wilcoxon's rank sum analysis to estimate the correlation of our signature with the 22 TICs. Then TICs with LUAD prognostic ability were screened out by our Cox model and Kaplan-Meier analysis. The intersection of the above positive factors was identified by us as candidate TICs that may be related to the prognostic ability of our signature.

Results

Patient characteristics

Figure 1 shows the flowchart of our study. **Table 1** details the clinical parameters of the patients included in each cohort of our study. In our research, the training cohort is used to train the signature, and the validation cohort is used to verify the signatures' accuracy and applicability. According to the screening criteria we set 500 LUADs from the TCGA-LUAD project that were included in the training cohort. Validation cohort one consists of 398 LUADs from the GSE72094 dataset, and validation cohort two consists of 442 LUADs from the GSE68465 dataset.

A cuproptosis-related ten-gene signature was generated

We found 2116 cuproptosis-related genes following our criteria, shown in Table S1. Our previously described approach led us to screen 45 cuproptosis-related genes for prognostic potential in the training cohort (Table S2). After putting these genes into a LASSO analysis for dimensionality reduction and refinement, the model displayed the highest power when containing ten genes (**Figure 2**). We present the coefficients for each gene in **Table 2**.

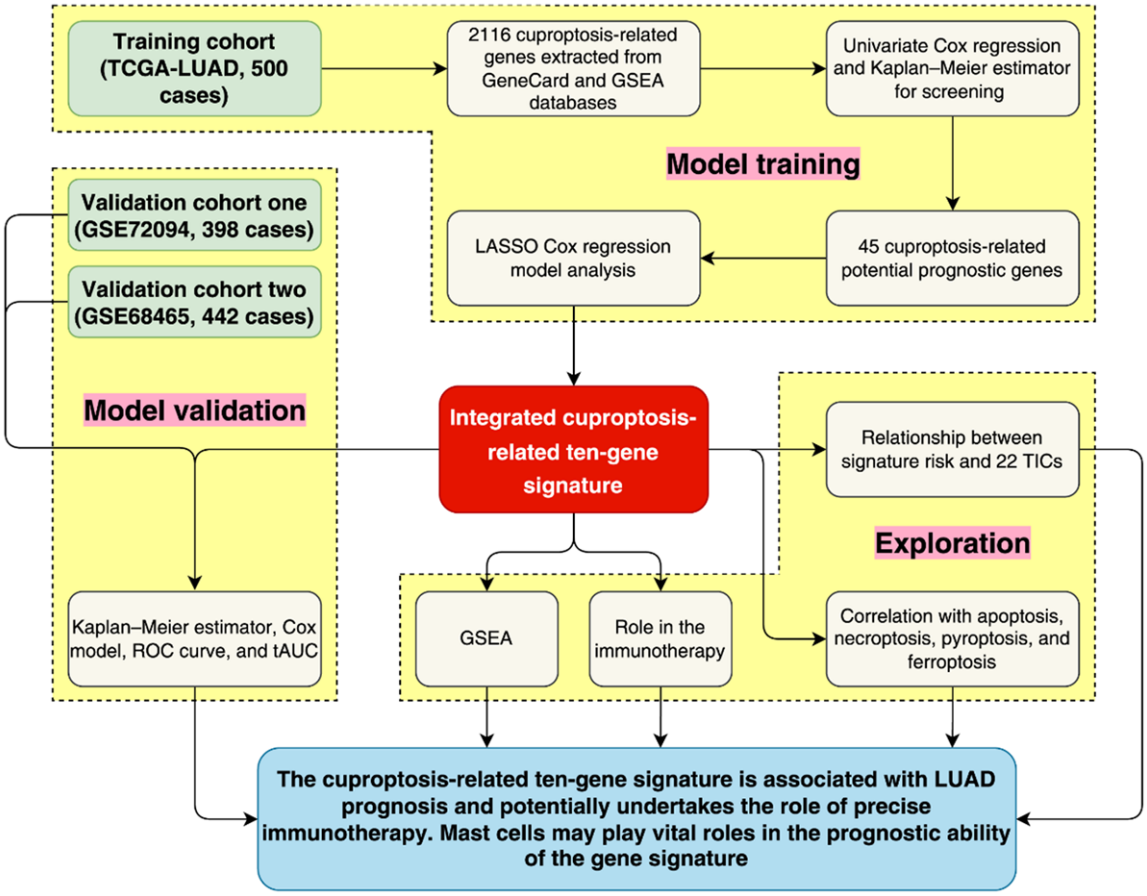

Figure 1. Research design and analysis process. TCGA: The Cancer Genome Atlas; LUAD: lung adenocarcinoma; LASSO: least absolute shrinkage and selection operator Cox regression model; ROC: receiver operating characteristic; AUC: Area under the ROC curve; tAUC: time-dependent AUC; GSEA: Gene Set Enrichment Analysis; TICs: tumor-infiltrating immune cells.

Table 1. Clinical characteristics of patients involved in the study

Characteristics	Training cohort (TCGA-LUAD, n = 500)	Validation cohort one (GSE72094, n = 398)	Validation cohort two (GSE68465, n = 442)
Age			
< 65	219 (43.8%)	107 (26.88%)	214 (48.42%)
≥ 65	271 (54.2%)	291 (73.12%)	228 (51.58%)
Unknown	10 (2%)	0	0
Gender			
Female	270 (54%)	222 (55.78%)	219 (49.55%)
Male	230 (46%)	176 (44.22%)	223 (50.45%)
Race			
White	386 (77.2%)	377 (94.72%)	294 (66.52%)
Non-White	60 (12%)	18 (4.52%)	19 (4.29%)
Unknown	54 (10.8%)	3 (0.75%)	129 (29.19%)
Ethnicity			
Hispanic or Latino	7 (1.4%)	9 (2.26%)	NA
Non-Hispanic or Latino	381 (76.2%)	381 (95.73%)	NA
Unknown	112 (22.4%)	8 (2.01%)	NA

Tumor stage			
Stage I	268 (53.6%)	254 (63.82%)	NA
Stage II	119 (23.8%)	67 (16.83%)	NA
Stage III	80 (16%)	57 (14.32%)	NA
Stage IV	25 (5%)	15 (3.77%)	NA
Unknown	8 (1.6%)	5 (1.26%)	NA
T classification			
T1	167 (33.4%)	NA	150 (33.94%)
T2	267 (53.4%)	NA	251 (56.79%)
T3	45 (9%)	NA	28 (6.33%)
T4	18 (3.6%)	NA	11 (2.49%)
Unknown	3 (0.6%)	NA	2 (0.45%)
Prior malignancy			
Yes	79 (15.8%)	NA	NA
No	421 (84.2%)	NA	NA
Tissue origin			
Upper lobe lung	291 (58.2%)	NA	NA
Non-upper lobe lung	209 (41.8%)	NA	NA
Smoking history			
Ever	415 (83%)	300 (75.38%)	300 (67.87%)
Never	71 (14.2%)	31 (7.79%)	49 (11.09%)
Unknown	14 (2.8%)	67 (16.83%)	93 (21.04%)
KRAS mutation			
Yes	NA	139 (34.92%)	NA
No	NA	259 (65.08%)	NA
TP53 mutation			
Yes	NA	97 (24.37%)	NA
No	NA	301 (75.63%)	NA
EGFR mutation			
Yes	NA	41 (10.3%)	NA
No	NA	357 (89.7%)	NA
STK11 mutation			
Yes	NA	64 (16.08%)	NA
No	NA	334 (83.92%)	NA
Vital status			
Alive	318 (63.6%)	285 (71.61%)	206 (46.61%)
Dead	182 (36.4%)	113 (28.39%)	236 (53.39%)

TCGA: The Cancer Genome Atlas; LUAD: lung adenocarcinoma.

The ten-gene signature proved to have stable prognostic capacity

We constructed three risk plots roughly representing our signature between the three cohorts (Figure S1). In the upper half of the plots, each dot represents a patient, ordered from left to right, by increasing risk score. The scatterplot in the middle of the plots shows the alive and dead status of the LUADs. The gene expression heatmap at the bottom of the plots shows the relative expression level of each gene included in our signature.

We calculated each LUAD's risk score using the formula described in the methods section, the coefficient of signature genes, and the relative expression of the relevant genes. In order to perform special approaches such as Kaplan-Meier analysis, patients will be stratified into

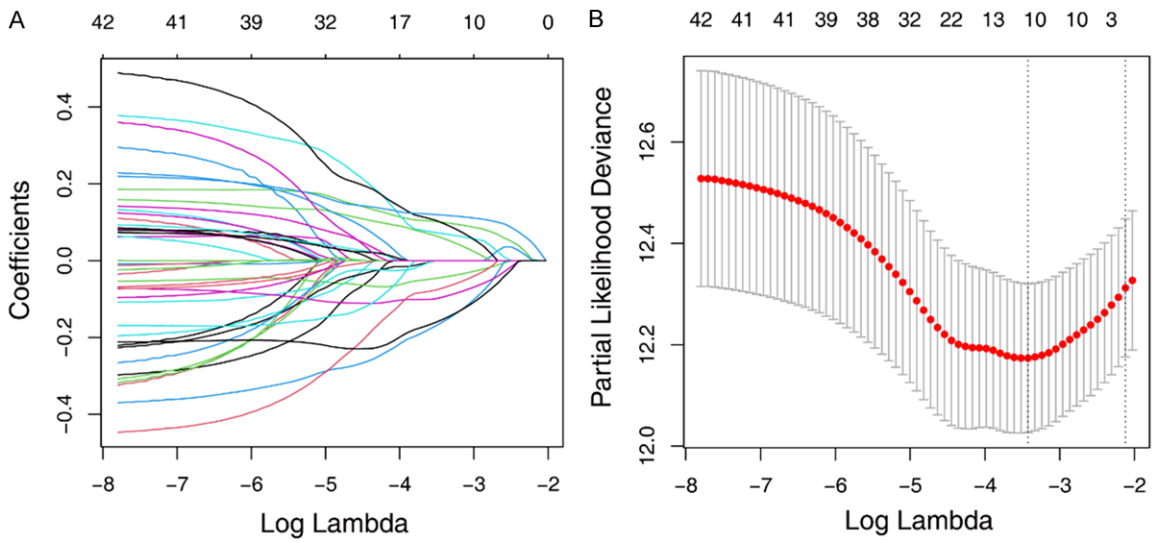

Figure 2. Development of a gene signature for prognosis prediction. A. LASSO coefficient profiles of 45 prognostic genes of LUAD. B. LASSO regression with ten-fold cross-validation obtained 45 prognostic genes using the minimum Lambda. LUAD: lung adenocarcinoma; LASSO: least absolute shrinkage and selection operator.

Table 2. Gene composition and coefficient of the signature obtained from the LASSO

Gene	Description	Coefficient
GJB3	Gap Junction Protein Beta 3	0.11847901
FKBP4	FKBP Prolyl Isomerase 4	0.099727149
XRCC5	X-Ray Repair Cross Complementing 5	0.097936761
CDKN3	Cyclin Dependent Kinase Inhibitor 3	0.070382376
GOLM1	Golgi Membrane Protein 1	0.058615651
AMT	Aminomethyltransferase	-0.043480013
RPS6KA1	Ribosomal Protein S6 Kinase A1	-0.071594933
MS4A1	Membrane Spanning 4-Domains A1	-0.095040152
PGPEP1	Pyroglutamyl-Peptidase I	-0.153370904
PEBP1	Phosphatidylethanolamine Binding Protein 1	-0.160078504

LASSO: least absolute shrinkage and selection operator.

high risk and low risk groups based on their median score. High-risk LUAD were less likely than low-risk LUAD to gain a better prognosis in the training cohort, according to Kaplan-Meier analysis (**Figure 3**). Furthermore, the Kaplan-Meier analysis results for validation cohort one and validation cohort two matched those for the training cohort. In addition, in Figure S2A, we displayed each of the ten gene's prognosis ability in the form of Kaplan-Meier curves using the three cohorts' data, showing that the GJB3, FKBP4, XRCC5, CDKN3, and GOLM1 performed stable unfavorable impact on LUAD patients, while AMT, RPS6KA1, MS4A1, PGPEP1, and PEBP1 helped the prognosis improvement of LUADs.

Our Cox analysis was mainly designed to determine whether the risk score could be classified as an independent risk factor for LUAD patient prognosis. Age, gender, race, ethnicity, tumor stage, tumor origin, and other clinical characteristics were included in the Cox model (**Figure 3D**). Univariate Cox regression results showed that risk score predicted LUAD outcome in all cohorts. The multivariate Cox analysis results showed that the risk score's hazard ratio was 3.837 (95% CI: 2.407-6.116, P = 1.59e-08) in the training cohort, 4.541 (95% CI: 2.624-7.861, P = 6.45e-08) in the validation cohort one, and 3.631 (95% CI: 2.193-6.011, P = 5.33e-07) in the validation cohort two. Based on these analyses, we found that the signature risk score could independently predict the prognosis of LUAD. In addition, the Cox regression showed the tumor stage of the training cohort and validation cohort one, the gender of validation cohort one, the age and T classification of validation cohort two also showed independent prognostic value, however, the risk score was stronger than them in terms of the *p*-value. Moreover, as shown in the chart exhibited in Figure S2B, the univariate Cox regression demonstrated that GJB3, FKBP4, XRCC5, CDKN3,

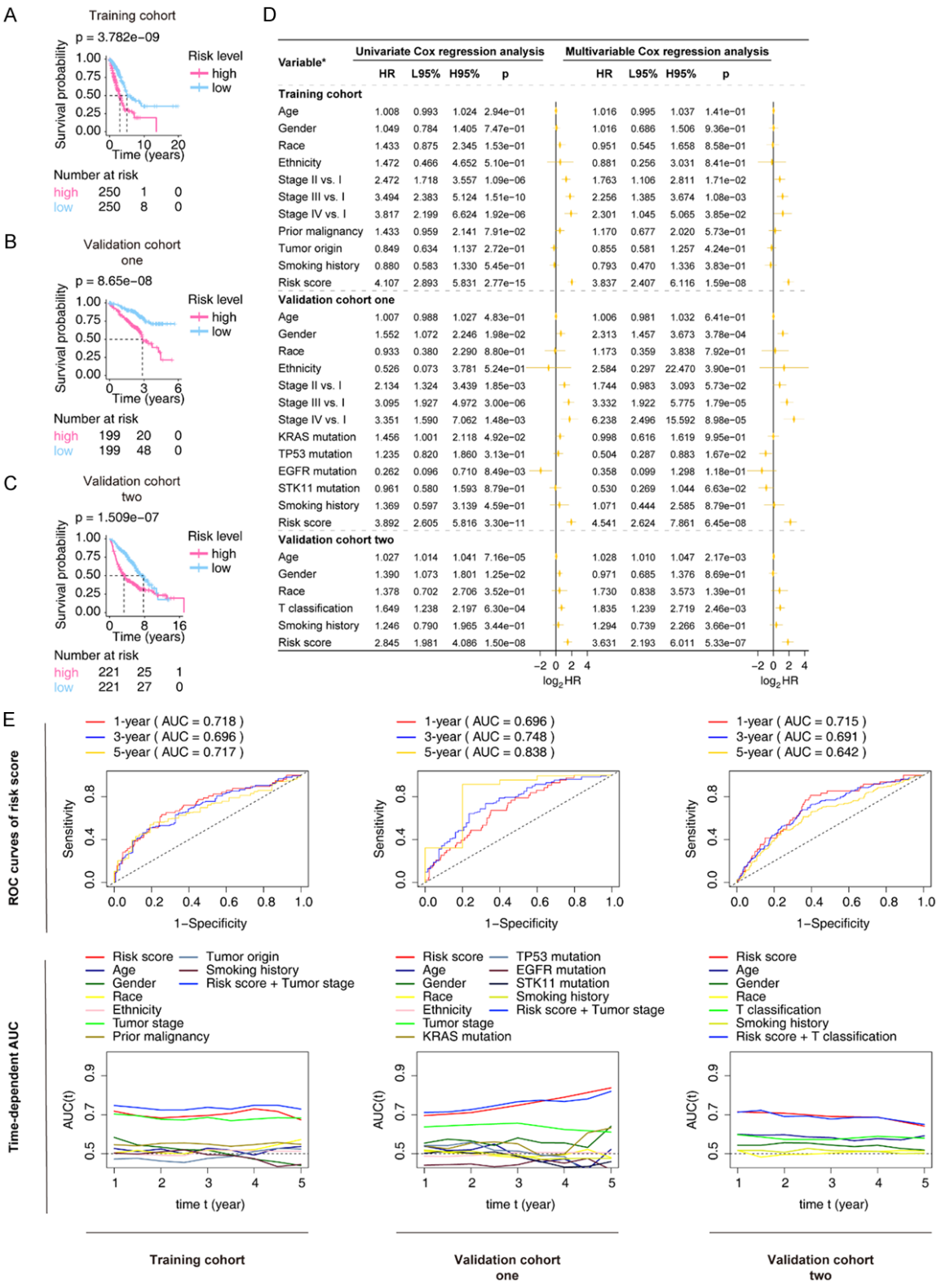

Figure 3. Validation of the ten-gene signature in three cohorts. A-C. Kaplan-Meier analysis. Patients in each cohort were divided into low-risk groups and high-risk groups based on their median risk score. The log-rank test with a *p*-value < 0.05 suggests the survival difference is significant. The bottom part displays the number of patients at risk. D. Univariate and multivariable Cox proportional hazards models. *: the variables involved in the studied cohorts, explains as follows: Gender: male vs. female; Race: white vs. non-white; Ethnicity: Hispanic or Latino vs.

non-Hispanic or Latino; Prior malignancy: yes vs. no; Tumor origin: upper lobe lung vs. non-upper lobe lung; Smoking history: ever vs. never; KRAS mutation: yes vs. no; TP53 mutation: yes vs. no; EGFR mutation: yes vs. no; STK11 mutation: yes vs. no; T classification: T2-T4 vs. T1. HR: hazard ratio; L95%: 95% confidence interval lower; H95%: 95% confidence interval higher; vs.: versus. E. ROC curves and tAUC. The ROC curves valued the accuracy for LUAD outcome prediction of our signature at 1-, 3-, and 5-year, respectively. The tAUC analyses compared our signature's prognostic ability with other available clinical characteristics. The larger the AUC, the stronger the model's predictive ability. HR: hazard ratio; CI: confidence interval; ROC: receiver operating characteristic; AUC: area under the ROC curve; tAUC: time-dependent AUC; LUAD: lung adenocarcinoma.

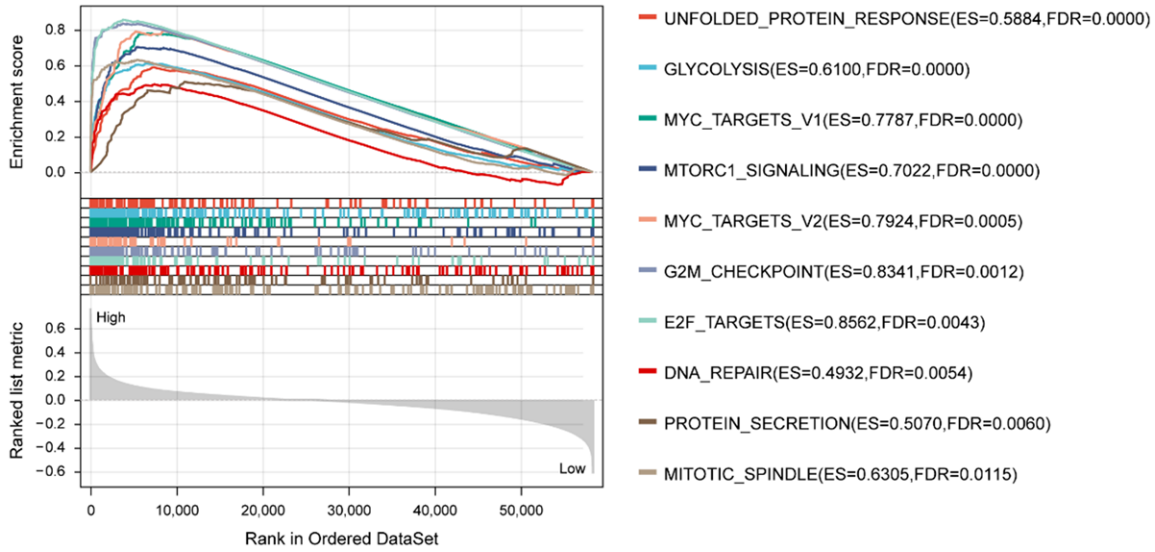

Figure 4. GSEA analysis with the HALLMARK gene set as the background identified relevant pathways of our signature. The significance threshold of this analysis was set as: *p*-value < 0.05, and FDR < 0.25. GSEA: Gene Set Enrichment Analysis; FDR: False Discovery Rate.

and GOLM1 impacted LUAD patients adversely, while AMT, RPS6KA1, MS4A1, PGPEP1, and PEBP1 contributed positively to LUADs' outcomes, which was consistent to the findings in the Kaplan-Meier curves.

The subsequent ROC analysis showed that the AUC of the signature in the training cohort was 0.718 at 1-year, 0.696 at 3-year, and 0.717 at 5-year, showing good predictive ability (**Figure 3E**). Our later tAUC results showed that the tumor stage surpassed our risk score around the 1.5-year time point and around the 5-year time point, but otherwise, the risk score performed at the best predictive level (**Figure 3E**). Interestingly, when we took the risk score and tumor stage combined, the predictive ability was stable beyond all factors at all time points, hinting that our signature was a favorable complement for the tumor stage. Notably, when we tested the AUC in the validation cohort one and two, the risk score showed a continuously better ability than any other factors, including tumor stage and T classification.

GSEA determined the mechanisms of the prognosis signature

Based on the median risk score, the LUADs were divided into high- and low-risk groups, and the prognosis of the two groups differed significantly. By analyzing the entire gene expression profile by GSEA, we explored the mechanism of the gene model. The unfolded protein response, glycolysis/gluconeogenesis, MYC, mTORC1 signaling, G2/M checkpoint, E2F transcription factors, DNA repair, protein secretion, and mitotic spindle assembly were the main enriched pathways identified by GSEA (**Figure 4** and Table S3).

The ten-gene signature's relationships with apoptosis, necroptosis, pyroptosis, and ferroptosis

We found apoptosis, necroptosis, pyroptosis, and ferroptosis genes followed our criteria, shown in Table S4. The Pearson coefficient examined the relationships between our prog-

nosis model and apoptosis, necroptosis, pyroptosis, and ferroptosis-related genes, respectively (Table S4 and Figure S3). The analysis showed that ANLN, GAPDH, CCNA2, SELENBP1, PLK1, CEP55, CCNB1, TUBA1C, KIF23, and TPX2 were the top ten correlated apoptosis-related genes, and overall, 2617/3681 (71.09%) genes significantly linked with the gene signature. FADD, CYLD, RIPK3, IPMK, ZBP1, CASP6, TNF, MAP3K7, TLR3, and PGLYRP1 were discovered as the top necroptosis-related that correlated with the ten-gene signature. As a whole, there were 13/20 (65%) necroptosis-related genes correlated with the signature pronouncedly. Moreover, the Pearson test found the top pyroptosis-related genes that correlated with our signature are NLRP1, CYCS, CARD8, CHMP2B, IL1A, ELANE, CASP3, CHMP4A, CHMP4C, and GSDMB. In total, 34/50 (68%) pyroptosis-related genes correlated with our signature. The examination found SLC2A1, RRM2, CDCA3, AURKA, VDAC2, EIF2S1, PEBP1, ISCU, EPT1, SIRT3 were top ferroptosis-related genes that correlated with our signature. To sum up, there were 245/380 (64.47%) ferroptosis-related genes correlating with our signature.

The role of risk score participating in immunotherapy

We explored the TMB difference among the risk score, and the Pearson coefficient found that the TMB was positively correlated with the risk score (**Figure 5A**). We found that the high risk score group had a high TMB based on our Wilcoxon test (**Figure 5B**). After receiving immune blockade therapy, many studies and clinical trials have shown that the higher the somatic TMB the patients have, the better treatment response, longer survival, and more clinical benefit, will present [47]. As our analyses indicate, our risk score may be as effective as TMB in determining immunotherapy efficacy and deserves further investigation.

The Pearson correlation analysis identified eight signatures, TBX2, GZMB, CXCL10, CD274, CTLA4, TNF, IFNG, and PRF1, significantly correlated with our risk score (**Figure 5**). As shown by a concurrent Wilcoxon analysis, six of 15 immune-relevant signatures, TNF, TBX2, GZMB, CXCL10, CTLA4, and CD274, showed significant differences between high-risk and low-risk groups (**Figure 5**). Incorporating the Wilcoxon and Pearson analyses, six genes, including TNF, TBX2, GZMB, CXCL10, CTLA4, and CD274, were closely connected to the ten-gene signature. Subsequently, we focused on the six identified immune relevant signatures. We tested these six signatures' prognosis roles in the high and low-risk groups to see the "comfort risk score zone" for potential immunotherapy. As shown in **Figure 5E**, the gene CD274 did not affect the prognosis of high-risk and low-risk LUAD. However, according to the *p*-value, the prognosis of the high-risk group may be more sensitive to the expression level of CD274, which seems to indicate that the high-risk group will have a stronger therapeutic response to CD274-targeted therapy. In subsequent analysis, we found that CTLA4 showed the same efficacy in protecting LUAD prognosis in high-risk and low-risk groups. If we observe the *p*-value more finely, we estimate that the high-risk group may be more sensitive to CTLA4 expression than the low-risk group. Moreover, high expression of CXCL10 and GZMB protected LUAD prognosis in the low-risk group but had no prognostic function in the high-risk group. TNF and TBX2 expression can affect the LUAD prognosis in the high-risk group but not in the low-risk group. These results hint that our risk score system could potentially guide immunotherapy choices based on each immune relevant signature's "comfort risk score zone", however, more clinical data are needed to support our conclusions.

It has been proposed that TIDE score can serve as a surrogate biomarker in predicting response to immune checkpoint blockades, such as anti-PD1 and anti-CTLA4 in NSCLC [43-45]. A high TIDE score indicates a higher likelihood of immune evasion, which means that a high TIDE score predicts less benefit from immunotherapy, while a low TIDE score predicts a greater benefit [43-45]. For our study, we analyzed TIDE and risk scores together to examine immunotherapy's potential clinical efficacy in subgroups based on risk scores. Based on the findings, our high-risk patients have a lower TIDE risk score, which means that immunotherapy could benefit them more (**Figure 5F** and **5G**). The TIDE findings here correspond with our "TMB difference" result, also are consistent to "comfort risk score zone" of CTLA4, CD274, TNF, and TBX2 mentioned above.

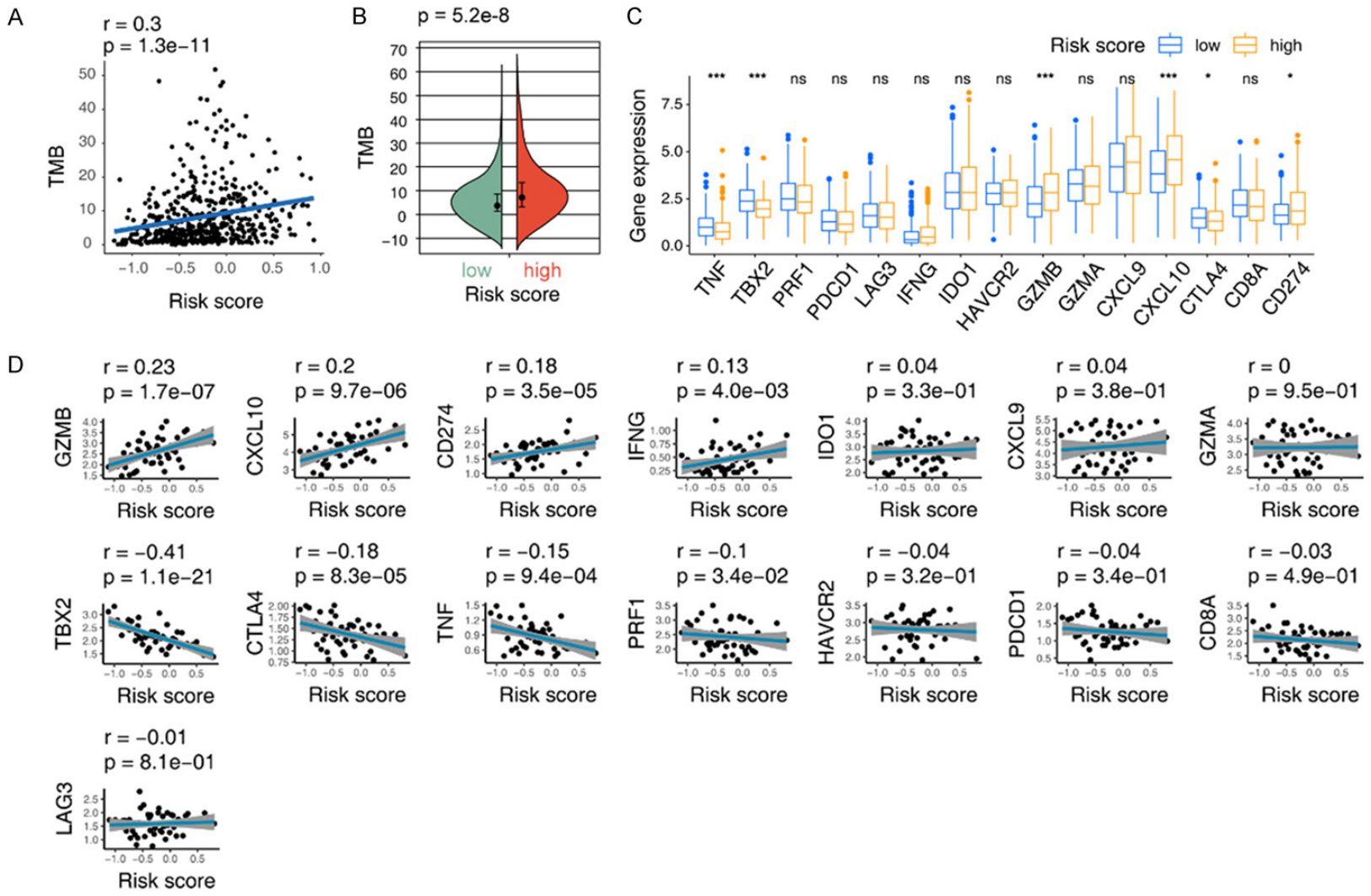
A
r = 0.3
p = 1.3e−11
TMB
Risk score
B
p = 5.2e-8
TMB
low
high
Risk score
C
Risk score
low
high
Gene expression
TNF
TBX2
PRF1
PDCD1
LAG3
IFNG
IDO1
HAVCR2
GZMB
GZMA
CXCL9
CXCL10
CTLA4
CD8A
CD274
D
r = 0.23
p = 1.7e−07
GZMB
r = 0.2
p = 9.7e−06
CXCL10
r = 0.18
p = 3.5e−05
CD274
r = 0.13
p = 4.0e−03
IFNG
r = 0.04
p = 3.3e−01
IDO1
r = 0.04
p = 3.8e−01
CXCL9
r = 0
p = 9.5e−01
GZMA
r = −0.41
p = 1.1e−21
TBX2
r = −0.18
p = 8.3e−05
CTLA4
r = −0.15
p = 9.4e−04
TNF
r = −0.1
p = 3.4e−02
PRF1
r = −0.04
p = 3.2e−01
HAVCR2
r = −0.04
p = 3.4e−01
PDCD1
r = −0.03
p = 4.9e−01
CD8A
r = −0.01
p = 8.1e−01
LAG3
Risk score

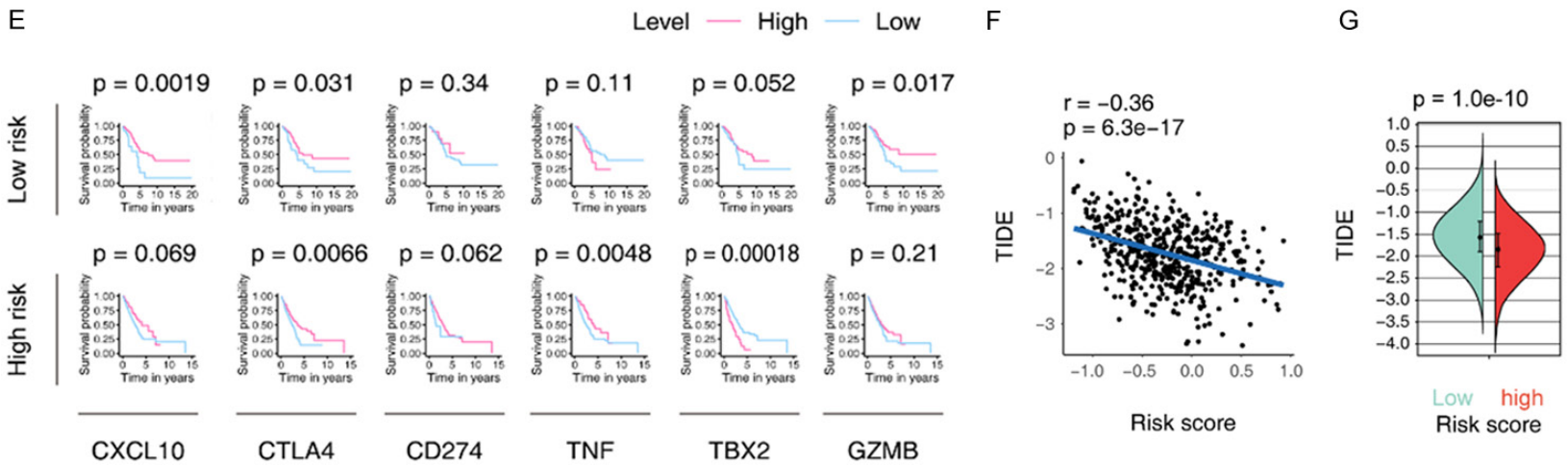

Figure 5. Determination of the relationship between the ten-gene signature and immunotherapy. A. The correlation between TMB and the signature tested by the Pearson coefficient. B. The TMB difference in the high and low-risk patients tested by the Wilcoxon rank-sum. C. The Wilcoxon rank-sum revealed the distribution differences of the immune relevant signatures in high and low-risk patients. ns: *P*-value > 0.05; *: *P*-value < 0.05; **: *P*-value < 0.01. D. The Pearson coefficient evaluated the correlations between the signature and the immune relevant signatures. E. The Kaplan-Meier estimator measured the immune relevant signatures' prognosis sensitive zone by testing in high and low-risk groups, respectively. F. The correlation between TIDE and the signature tested by the Pearson coefficient. G. The TIDE difference in the high and low-risk patients tested by the Wilcoxon rank-sum. *P*-value < 0.05 was considered statistically significant; TMB: Tumor mutational burden; TIDE: Tumor Immune Dysfunction and Exclusion.

Mast cells' vital roles in the ten-gene signature's prediction ability

Figure S4A details the distribution of the 22 TICs in each patient and high and low-risk groups. Figure S4B shows the mutual internal relationships of the 22 TICs in the LUADs. As shown in **Figure 6** and Table S5, the Wilcoxon rank sum test identified 13 TICs related to the risk score, and Pearson coefficient found 16 TICs closely linked to our signature. In summary, a total of 12 TICs are significantly related to the gene signature, which included Mast cells resting, T cells CD4 memory activated, Neutrophils, T cells CD4 memory resting, B cells memory, Macrophages M0, T cells CD8, Mast cells activated, Monocytes, Macrophages M1, T cells regulatory (Tregs), and Plasma cells. Specifically, our signature was positively correlated with T cells CD4 memory activated, Neutrophils, Macrophages M0, T cells CD8, Mast cells activated, and Macrophages M1, while it was correlated with the rest negatively.

In Figure S4, we show the portraits of 22 TICs in the training cohort and the correlations between them. We found that 13 types of TICs differed significantly in distribution between high-risk and low-risk groups based on Wilcoxon rank sum tests (**Figure 6** and Table S5). The results of Pearson coefficient analysis showed that there were 16 types of TICs associated with the risk score of our studies patients (**Figure 6** and Table S5). Using a Venn diagram, we summarized the above results and found that a total of 12 TICs included Mast cells resting, T cells CD4 memory activated, Neutrophils, T cells CD4 memory resting, B cells memory, Macrophages M0, T cells CD8, Mast cells activated, Monocytes, Macrophages M1, T cells regulatory (Tregs), and Plasma cells, were strongly associated with our signature. We found that our signature had a positive correlation with T cells CD4 memory activated, Neutrophils, Macrophages M0, T cells CD8, Mast cells activated, and Macrophages M1, and a negative correlation with the rest of the cell types based on Wilcoxon rank sums and Pearson analysis.

Our next step was to determine the survival predictive power of each of the 22 TICs using Cox regression and Kaplan-Meier curves. As shown in **Figure 7A**, Cox analysis can tell that Mast cells resting (HR = 0.764, 95% CI = 0.645-0.905, P = 1.84e-03) and Mast cells activated (HR = 1.141, 95% CI = 1.019-1.279, P = 2.25e-02) significantly affected the LUAD prognosis. LUAD's survival probability was significantly affected by Mast cells resting, Mast cells activated, and Dendritic cells resting as shown in the built Kaplan-Meier analysis (**Figure 7B**; Table S6). On the whole, the survival predictive analysis suggested the Mast cells resting and Mast cells activated pronounced closely connected to LUAD outcomes.

In summary, we adopted a combined approach of multiple analyzes in this section, and finally found TICs that were significantly associated with our gene signature and could predict the prognosis of LUAD, namely Mast cells resting and Mast cells activated. Our study suggests that mast cell infiltration may be key to the prognostic power of our gene signature.

Discussion

With the development of an effective classifier for LUAD, patients can be stratified based on their risk and prognosis on a targeted basis, which can maximize treatment efficacy and facilitate timely follow-up. In the present research, we innovatively adopting the novel cuproptosis concept to establish a cuproptosis-related ten-gene signature predicting LUAD outcomes by analyzing TCGA and GEO cohorts. Particularly, our freshness lay in adopting comprehensive bioinformatics analysis, including LASSO regression, Kaplan-Meier curves, Cox models, ROC curves, tAUC, and the validations in two independent datasets. Most importantly, we detailed the role of risk score participating in immunotherapy. We demonstrated at the end of the study that mast cell infiltration may have contributed to the prognostic power of the signature.

Regulated cell death is a pervasive process in organisms and critical for tissue homeostasis or restoring biological homeostasis after stress; it functions to eliminate useless or potentially dangerous cells [48]. Various heavy metals can induce regulated cell death through different subprograms. Tsvetkov and colleagues identified cuproptosis, a new form of cell death caused by copper accumulation in cells, in a recent study in *Science* [9, 10, 49]. In their study, they demonstrated that cuproptosis dif-

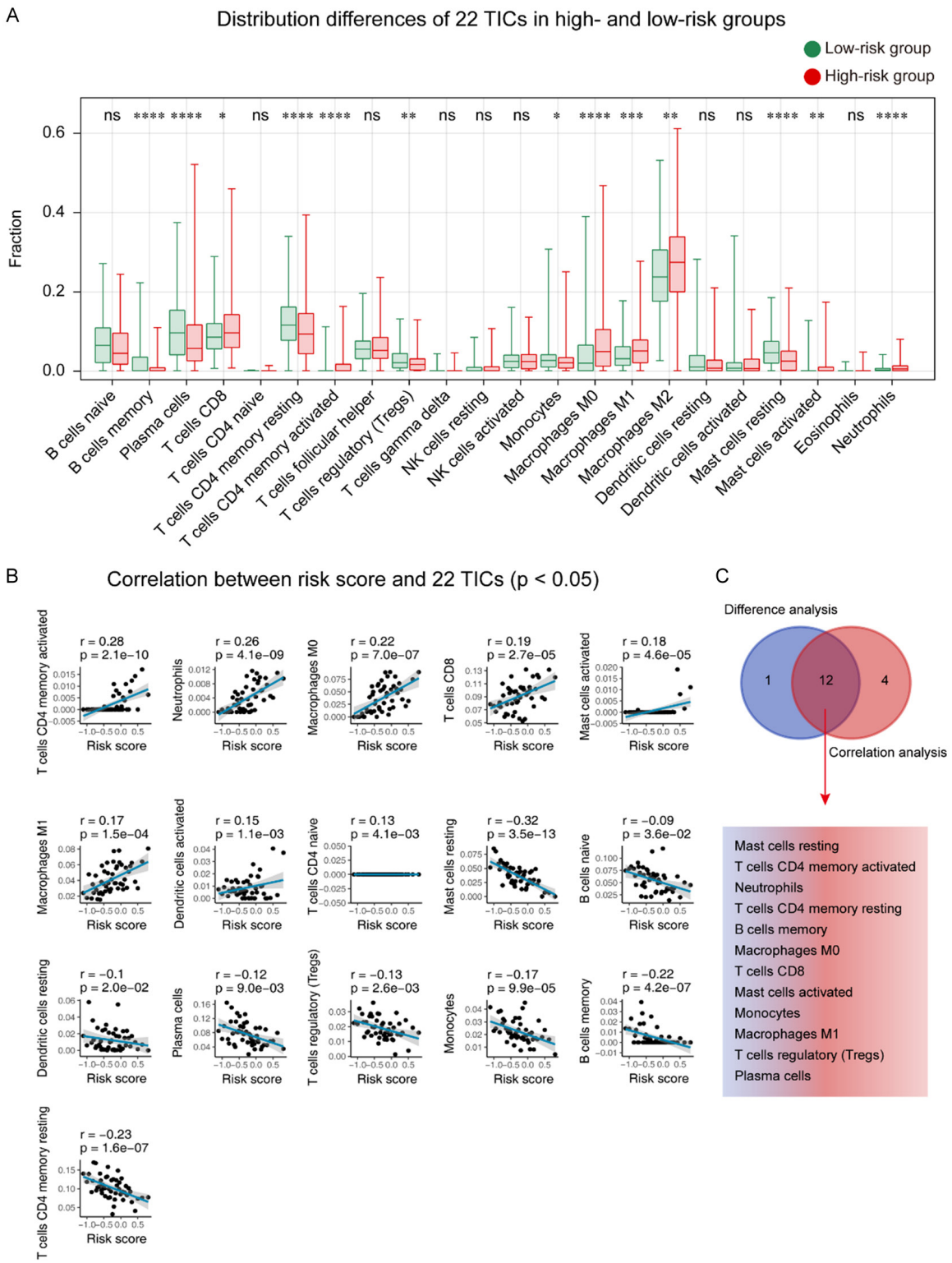

Figure 6. Comprehensive analysis determined the relationship between 22 TICs and the ten-gene signature. A. Patients were grouped according to their median risk score, and the Wilcoxon rank-sum was applied to detect the difference in TIC distribution between the high and low-risk groups. ns: *p*-value > 0.05; *: *p*-value < 0.05; **: *p*-value < 0.01; ***: *p*-value < 0.001; ****: *p*-value < 0.0001. B. The Pearson coefficient examined the correlations between TICs and our signature. Here, we only plotted the TIC correlation with a *p*-value < 0.05. C. The results of Wilcoxon's rank-sum test and the Pearson coefficient were intersected to determine stable and critical TICs. TIC: tumor-infiltrating immune cell; *p*-value < 0.05 is considered significant.

A

Variable	HR	Lower 95% CI	Upper 95% CI	P–value
Mast cells resting	0.764	0.645	0.905	1.84e–03
Monocytes	0.875	0.740	1.035	1.19e–01
Dendritic cells resting	0.879	0.743	1.039	1.31e–01
B cells memory	0.886	0.748	1.050	1.63e–01
Plasma cells	0.925	0.796	1.076	3.14e–01
NK cells activated	0.953	0.826	1.098	5.03e–01
T cells regulatory (Tregs)	0.970	0.843	1.116	6.72e–01
B cells naive	0.971	0.842	1.121	6.90e–01
T cells follicular helper	0.987	0.852	1.144	8.62e–01
T cells gamma delta	0.992	0.840	1.173	9.28e–01
T cells CD4 memory resting	1.013	0.871	1.179	8.66e–01
NK cells resting	1.014	0.876	1.173	8.54e–01
T cells CD8	1.017	0.876	1.180	8.27e–01
T cells CD4 memory activated	1.058	0.919	1.218	4.34e–01
Neutrophils	1.077	0.940	1.233	2.88e–01
T cells CD4 naive	1.078	0.990	1.172	8.24e–02
Eosinophils	1.088	0.965	1.226	1.67e–01
Macrophages M2	1.089	0.942	1.259	2.47e–01
Macrophages M1	1.091	0.957	1.244	1.92e–01
Dendritic cells activated	1.095	0.944	1.269	2.31e–01
Macrophages M0	1.135	0.988	1.303	7.32e–02
Mast cells activated	1.141	1.019	1.279	2.25e–02

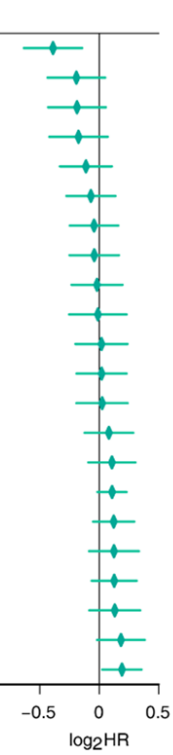

B

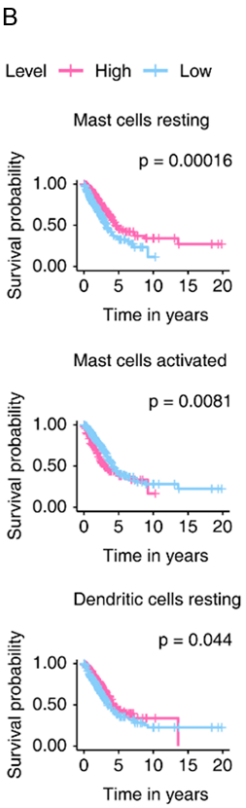

Figure 7. Prognosis ability assessment for the 22 TICs. A. We performed Cox analysis to determine the survival predicting power for the 22 TICs. Bold words indicate *p*-values < 0.05. B. Kaplan-Meier estimators were plotted to check the TICs that differ in the survival possibility between low and high-risk groups. Only showed Kaplan-Meier curves with *p*-values < 0.05. HR: hazard ratio; TIC: tumor-infiltrating immune cell; *p*-value < 0.05 is considered significant.

fers from other forms of death [9, 50], including apoptosis [4], necroptosis [5], pyroptosis [6], and ferroptosis [7, 8]. Copper is involved in many physiological processes, and studies have reported that disturbance of copper homeostasis can lead to structural abnormalities or loss of some basic physiological functions, and studies have also shown that copper homeostasis is deregulated in many cancers [51]. Copper plays an vital part in carcinogenesis and metastases progression and therapeutic resistance [10]. It is worth noting that recent research has provided an in-depth understanding of copper metabolism, and as a result, many therapeutic strategies have been developed against this metal [10]. Copper metabolism has been extensively studied over the years, but some "uncharted territory" remains, especially copper metabolism and lung adenocarcinoma. Our study aimed to construct a cuproptosis-related prognostic model to predict lung adenocarcinoma prognosis, uncover the "uncharted territory", and provide more clues for further research.

While the way of regulated cell death of cuproptosis, apoptosis, necroptosis, pyroptosis, and ferroptosis varies [9, 50], from our research, they seem to be somewhat related, such as our cuproptosis-related signature correlated with 2617/3681 (71.09%) apoptosis-related genes,13/20 (65%) necroptosis-related genes, 34/50 (68%) pyroptosis-related genes, and 245/380 (64.47%) ferroptosis-related genes, providing potential interpretations and encouragements for upcoming research of cell death-related tumor mechanism.

Our risk model contains ten genes (**Table 2**), which were GJB3, FKBP4, XRCC5, CDKN3, GOLM1, AMT, RPS6KA1, MS4A1, PGPEP1, and PEBP1. Our study confirmed that GJB3, FKBP4, XRCC5, CDKN3, and GOLM1 had disruptive effects on LUAD prognosis, whereas the remaining genes showed protective effects

(Figure S2). GJB3 is a member of the connexin gene family [52]. An earlier study identified GJB3 as a gene associated with poor prognosis in LUAD by Aasen and colleagues [52]. It has been reported that FKBP4 binds to various cellular receptors or targets in cancer [53]. FKBP4 is highly expressed in LUAD tissues and is closely associated with tumor size [54]. According to Du and colleagues, XRCC5 prevents copper from oxidizing DNA [55]. It has been reported that XRCC5 is involved in developing several tumors, including lung cancer [56]. Researchers found CDKN3 overexpression is associated with a poorer prognosis in LUAD patients, where CDKN3 plays an important role in cell division and tumor progression [57, 58]. According to Song's group, GOLM1 can promote various cancer types' oncogenic phenotypes, promoting proliferation, migration, and invasion of lung cancer cells [59].

Gene signature functions are influenced by pathways involving unfolded protein response, glycolysis/gluconeogenesis, and MYC, according to GSEA. The unfolded protein response is associated with many diseases, including cancer. In non-small cell lung cancer cells [60], Zhao et al. demonstrated that unfolded protein response promotes doxorubicin-induced apoptosis [61]. Glycolysis is an inefficient form of energy metabolism. Recent studies have demonstrated that shortened gluconeogenesis can partially avoid the need for glycolysis in lung cancer cells. Inhibiting glycolysis is considered a way to treat lung cancer. By activating cell cycle kinesins and regulating metabolism, MYC regulates lung cancer cell growth, resistance, death, and dissemination [62]. For patients with lung cancer, novel MYC inhibition strategies may provide new treatment options [62].

Cancer immunotherapy prolongs the survival of cancer patients and as more cancer patients become eligible for immune-based cancer treatments, revealing that this approach is revolutionizing the field of oncology [63, 64]. New therapeutic combinations and newly discovered drug targets are expanding the use of immunotherapy in cancer treatment [63, 64]. This study gives hints about which immunotherapy targets to use and under what circumstances to apply them. We first found that our risk score was associated with TMB, suggesting that our signature appeared to guide immunotherapy. Next, we followed the trail and found six targets related to our score, including TNF, TBX2, GZMB, CXCL10, CTLA4, and CD274. We analyzed the sensitivity of each target in different risk score intervals and found that the targeting of CXCL10 and GZMB was more effective in low-risk patients, and triggering CTLA4, CD274, TNF, and TBX2 can benefit the high-risk group more. Additionally, the TIDE database confirmed the above points of view and affirmed that our risk score could bring hope to precisely targeted therapy.

Our analysis of TICs concluded that mast cells might be able to provide secure prognostic power for our signature. As an essential stromal component of the immune system, mast cells play a vital role in the immune microenvironment in the progression of malignant tumors [65-68]. Mast cells can promote growth factor secretion, which may be associated with poor prognosis in NSCLC [68]. In recent years, evidence has revealed the involvement of mast cells in the progression of LUAD [68]. Further research on mast cells' role in tumor microenvironment remodeling and tumor immunity should be conducted since the current research results are not sufficient.

Several limitations are present in this study. Retrospective data was used to generate this ten-gene signature. Although it has been confirmed to have stable prognosis ability through being applied to another two independent cohorts, its corroboration source was obtained from public databases. Its clinical applicability needs further confirmation with more prospective data. Furthermore, there are still no wet-lab experimental facts to hold up the prognostic power of the ten genes and their parts in cuproptosis-related mechanisms and immune infiltration. More *in vitro* and *in vivo* research is therefore needed to unveil more clues about the future potential of the ten-gene signature.

Conclusion

A ten-gene prognostic signature associated with cuproptosis in LUAD was constructed in this study. Its stability and applicability was confirmed by applying it to independent cohorts. The risk model we developed has the potential to take on the role of precision immunotherapy. According to the immune infiltration analysis, mast cells might contribute to main-

taining the signature's predictive ability. Our work may advance the development of LUAD diagnosis and treatment.

Disclosure of conflict of interest

None.

Abbreviations

LUAD, lung adenocarcinoma; LASSO, least absolute shrinkage and selection operator Cox regression model; TCGA, The Cancer Genome Atlas; ROC, receiver operating characteristic; AUC, Area under the ROC curve; tAUC, Time-dependent AUC; GSEA, Gene Set Enrichment Analysis; TICs, tumor-infiltrating immune cells; HR, hazard ratio; CI, confidence interval; FDR, False Discovery Rate; TIDE, Tumor Immune Dysfunction and Exclusion.

Address correspondence to: Yao Cui, Department of Oncology, Henan Provincial People's Hospital, People's Hospital of Zhengzhou University, Henan University People's Hospital, Zhengzhou 450003, Henan, China. ORCID: 0000-0003-0273-9178; E-mail: ebia@qq.com

References

[1] Siegel RL, Miller KD, Fuchs HE and Jemal A. Cancer statistics, 2021. CA Cancer J Clin 2021; 71: 7-33.

[2] Oskarsdottir GN, Bjornsson J, Jonsson S, Isaksson HJ and Gudbjartsson T. Primary adenocarcinoma of the lung--histological subtypes and outcome after surgery, using the IASLC/ATS/ERS classification of lung adenocarcinoma. APMIS 2016; 124: 384-392.

[3] Strasser A and Vaux DL. Cell death in the origin and treatment of cancer. Mol Cell 2020; 78: 1045-1054.

[4] Wu X, Kong W, Qi X, Wang S, Chen Y, Zhao Z, Wang W, Lin X, Lai J, Yu Z and Lai G. Icariin induces apoptosis of human lung adenocarcinoma cells by activating the mitochondrial apoptotic pathway. Life Sci 2019; 239: 116879.

[5] Lu Y, Luo X, Wang Q, Chen J, Zhang X, Li Y, Chen Y, Li X and Han S. A novel necroptosis-related lncRNA signature predicts the prognosis of lung adenocarcinoma. Front Genet 2022; 13: 862741.

[6] Lin W, Chen Y, Wu B, Chen Y and Li Z. Identification of the pyroptosisrelated prognostic gene signature and the associated regulation axis in lung adenocarcinoma. Cell Death Discov 2021; 7: 161.

[7] Ma C, Li F and Luo H. Prognostic and immune implications of a novel ferroptosis-related tengene signature in lung adenocarcinoma. Ann Transl Med 2021; 9: 1058.

[8] Zhang A, Yang J, Ma C, Li F and Luo H. Development and validation of a robust ferroptosis-related prognostic signature in lung adenocarcinoma. Front Cell Dev Biol 2021; 9: 616271.

[9] Tsvetkov P, Coy S, Petrova B, Dreishpoon M, Verma A, Abdusamad M, Rossen J, Joesch-Cohen L, Humeidi R, Spangler RD, Eaton JK, Frenkel E, Kocak M, Corsello SM, Lutsenko S, Kanarek N, Santagata S and Golub TR. Copper induces cell death by targeting lipoylated TCA cycle proteins. Science 2022; 375: 1254-1261.

[10] Tang D, Chen X and Kroemer G. Cuproptosis: a copper-triggered modality of mitochondrial cell death. Cell Res 2022; 32: 417-418.

[11] Ma C, Li F, He Z and Zhao S. A more novel and powerful prognostic gene signature of lung adenocarcinoma determined from the immune cell infiltration landscape. Front Surg 2022; 9: 1015263.

[12] Ma C, Li F, Wang Z and Luo H. A novel immune-related gene signature predicts prognosis of lung adenocarcinoma. Biomed Res Int 2022; 2022: 4995874.

[13] Zheng X, Li Y, Ma C, Zhang J, Zhang Y, Fu Z and Luo H. Independent prognostic potential of GNPNAT1 in lung adenocarcinoma. Biomed Res Int 2020; 2020: 8851437.

[14] Ma C, Luo H, Cao J, Gao C, Fa X and Wang G. Independent prognostic implications of RRM2 in lung adenocarcinoma. J Cancer 2020; 11: 7009-7022.

[15] Ma C, Luo H, Cao J, Zheng X, Zhang J, Zhang Y and Fu Z. Identification of a novel tumor microenvironment-associated eight-gene signature for prognosis prediction in lung adenocarcinoma. Front Mol Biosci 2020; 7: 571641.

[16] Li X, Ma C, Luo H, Zhang J, Wang J and Guo H. Identification of the differential expression of genes and upstream microRNAs in small cell lung cancer compared with normal lung based on bioinformatics analysis. Medicine (Baltimore) 2020; 99: e19086.

[17] Wang Z, Jensen MA and Zenklusen JC. A practical guide to the cancer genome atlas (TCGA). Methods Mol Biol 2016; 1418: 111-141.

[18] Clough E and Barrett T. The gene expression omnibus database. Methods Mol Biol 2016; 1418: 93-110.

[19] Friedman J, Hastie T and Tibshirani R. Regularization paths for generalized linear models via coordinate descent. J Stat Softw 2010; 33: 1-22.

[20] Goeman JJ. L1 penalized estimation in the Cox proportional hazards model. Biom J 2010; 52: 70-84.

[21] Sauerbrei W, Royston P and Binder H. Selection of important variables and determination

of functional form for continuous predictors in multivariable model building. Stat Med 2007; 26: 5512-5528.
[22] Tibshirani R. The lasso method for variable selection in the Cox model. Stat Med 1997; 16: 385-395.
[23] Cao R and Lopez-de-Ullibarri I. ROC curves for the statistical analysis of microarray data. Methods Mol Biol 2019; 1986: 245-253.
[24] Subramanian A, Tamayo P, Mootha VK, Mukherjee S, Ebert BL, Gillette MA, Paulovich A, Pomeroy SL, Golub TR, Lander ES and Mesirov JP. Gene set enrichment analysis: a knowledge-based approach for interpreting genome-wide expression profiles. Proc Natl Acad Sci U S A 2005; 102: 15545-15550.
[25] Liberzon A, Subramanian A, Pinchback R, Thorvaldsdottir H, Tamayo P and Mesirov JP. Molecular signatures database (MSigDB) 3.0. Bioinformatics 2011; 27: 1739-1740.
[26] Zhou N and Bao J. FerrDb: a manually curated resource for regulators and markers of ferroptosis and ferroptosis-disease associations. Database (Oxford) 2020; 2020: baaa021.
[27] Chalmers ZR, Connelly CF, Fabrizio D, Gay L, Ali SM, Ennis R, Schrock A, Campbell B, Shlien A, Chmielecki J, Huang F, He Y, Sun J, Tabori U, Kennedy M, Lieber DS, Roels S, White J, Otto GA, Ross JS, Garraway L, Miller VA, Stephens PJ and Frampton GM. Analysis of 100,000 human cancer genomes reveals the landscape of tumor mutational burden. Genome Med 2017; 9: 34.
[28] Fabrizio FP, Trombetta D, Rossi A, Sparaneo A, Castellana S and Muscarella LA. Gene code CD274/PD-L1: from molecular basis toward cancer immunotherapy. Ther Adv Med Oncol 2018; 10: 1758835918815598.
[29] Rowshanravan B, Halliday N and Sansom DM. CTLA-4: a moving target in immunotherapy. Blood 2018; 131: 58-67.
[30] Holderried TAW, de Vos L, Bawden EG, Vogt TJ, Dietrich J, Zarbl R, Bootz F, Kristiansen G, Brossart P, Landsberg J and Dietrich D. Molecular and immune correlates of TIM-3 (HAVCR2) and galectin 9 (LGALS9) mRNA expression and DNA methylation in melanoma. Clin Epigenetics 2019; 11: 161.
[31] Platten M, von Knebel Doeberitz N, Oezen I, Wick W and Ochs K. Cancer immunotherapy by targeting IDO1/TDO and their downstream effectors. Front Immunol 2015; 5: 673.
[32] Andrews LP, Marciscano AE, Drake CG and Vignali DA. LAG3 (CD223) as a cancer immunotherapy target. Immunol Rev 2017; 276: 80-96.
[33] Ribas A and Wolchok JD. Cancer immunotherapy using checkpoint blockade. Science 2018; 359: 1350-1355.
[34] Raskov H, Orhan A, Christensen JP and Gogenur I. Cytotoxic CD8(+) T cells in cancer and cancer immunotherapy. Br J Cancer 2021; 124: 359-367.
[35] Shi Z, Shen J, Qiu J, Zhao Q, Hua K and Wang H. CXCL10 potentiates immune checkpoint blockade therapy in homologous recombination-deficient tumors. Theranostics 2021; 11: 7175-7187.
[36] Liang YK, Deng ZK, Chen MT, Qiu SQ, Xiao YS, Qi YZ, Xie Q, Wang ZH, Jia SC, Zeng and Lin HY. CXCL9 is a potential biomarker of immune infiltration associated with favorable prognosis in ER-negative breast cancer. Front Oncol 2021; 11: 710286.
[37] Inoue H, Park JH, Kiyotani K, Zewde M, Miyashita A, Jinnin M, Kiniwa Y, Okuyama R, Tanaka R, Fujisawa Y, Kato H, Morita A, Asai J, Katoh N, Yokota K, Akiyama M, Ihn H, Fukushima S and Nakamura Y. Intratumoral expression levels of PD-L1, GZMA, and HLA-A along with oligoclonal T cell expansion associate with response to nivolumab in metastatic melanoma. Oncoimmunology 2016; 5: e1204507.
[38] Hurkmans DP, Basak EA, Schepers N, Oomen-De Hoop E, Van der Leest CH, El Bouazzaoui S, Bins S, Koolen SLW, Sleijfer S, Van der Veldt AAM, Debets R, Van Schaik RHN, Aerts J and Mathijssen RHJ. Granzyme B is correlated with clinical outcome after PD-1 blockade in patients with stage IV non-small-cell lung cancer. J Immunother Cancer 2020; 8: e000586.
[39] Jorgovanovic D, Song M, Wang L and Zhang Y. Roles of IFN-gamma in tumor progression and regression: a review. Biomark Res 2020; 8: 49.
[40] Fan C, Hu H, Shen Y, Wang Q, Mao Y, Ye B and Xiang M. PRF1 is a prognostic marker and correlated with immune infiltration in head and neck squamous cell carcinoma. Transl Oncol 2021; 14: 101042.
[41] Li C, Pan J, Jiang Y, Yu Y, Jin Z and Chen X. Characteristics of the immune cell infiltration landscape in gastric cancer to assistant immunotherapy. Front Genet 2022; 12: 793628.
[42] Freeman AJ, Kearney CJ, Silke J and Oliaro J. Unleashing TNF cytotoxicity to enhance cancer immunotherapy. Trends Immunol 2021; 42: 1128-1142.
[43] Chen Y, Li ZY, Zhou GQ and Sun Y. An immune-related gene prognostic index for head and neck squamous cell carcinoma. Clin Cancer Res 2021; 27: 330-341.
[44] Fu J, Li K, Zhang W, Wan C, Zhang J, Jiang P and Liu XS. Large-scale public data reuse to model immunotherapy response and resistance. Genome Med 2020; 12: 21.
[45] Jiang P, Gu S, Pan D, Fu J, Sahu A, Hu X, Li Z, Traugh N, Bu X, Li B, Liu J, Freeman GJ, Brown MA, Wucherpfennig KW and Liu XS. Signatures

of T cell dysfunction and exclusion predict cancer immunotherapy response. Nat Med 2018; 24: 1550-1558.
[46] Ye L, Zhang T, Kang Z, Guo G, Sun Y, Lin K, Huang Q, Shi X, Ni Z, Ding N, Zhao KN, Chang W, Wang J, Lin F and Xue X. Tumor-infiltrating immune cells act as a marker for prognosis in colorectal cancer. Front Immunol 2019; 10: 2368.
[47] Strickler JH, Hanks BA and Khasraw M. Tumor mutational burden as a predictor of immunotherapy response: is more always better? Clin Cancer Res 2021; 27: 1236-1241.
[48] Tang D, Kang R, Berghe TV, Vandenabeele P and Kroemer G. The molecular machinery of regulated cell death. Cell Res 2019; 29: 347-364.
[49] Ge EJ, Bush AI, Casini A, Cobine PA, Cross JR, DeNicola GM, Dou QP, Franz KJ, Gohil VM, Gupta S, Kaler SG, Lutsenko S, Mittal V, Petris MJ, Polishchuk R, Ralle M, Schilsky ML, Tonks NK, Vahdat LT, Van Aelst L, Xi D, Yuan P, Brady DC and Chang CJ. Connecting copper and cancer: from transition metal signalling to metalloplasia. Nat Rev Cancer 2022; 22: 102-113.
[50] Chen X, Kang R, Kroemer G and Tang D. Broadening horizons: the role of ferroptosis in cancer. Nat Rev Clin Oncol 2021; 18: 280-296.
[51] Lelievre P, Sancey L, Coll JL, Deniaud A and Busser B. The multifaceted roles of copper in cancer: a trace metal element with dysregulated metabolism, but also a target or a bullet for therapy. Cancers (Basel) 2020; 12: 3594.
[52] Aasen T, Sansano I, Montero MA, Romagosa C, Temprana-Salvador J, Martinez-Marti A, Moline T, Hernandez-Losa J and Ramon y Cajal S. Insight into the role and regulation of gap junction genes in lung cancer and identification of nuclear Cx43 as a putative biomarker of poor prognosis. Cancers (Basel) 2019; 11: 320.
[53] Xiong H, Chen Z, Lin B, Xie B, Liu X, Chen C, Li Z, Jia Y, Wu Z, Yang M, Jia Y, Wang L, Zhou J and Meng X. Naringenin regulates FKBP4/NR3C1/NRF2 axis in autophagy and proliferation of breast cancer and differentiation and maturation of dendritic cell. Front Immunol 2021; 12: 745111.
[54] Meng W, Meng J, Jiang H, Feng X, Wei D and Ding Q. FKBP4 accelerates malignant progression of non-small-cell lung cancer by activating the Akt/mTOR signaling pathway. Anal Cell Pathol (Amst) 2020; 2020: 6021602.
[55] Du T, Caragounis A, Parker SJ, Meyerowitz J, La Fontaine S, Kanninen KM, Perreau VM, Crouch PJ and White AR. A potential copper-regulatory role for cytosolic expression of the DNA repair protein XRCC5. Free Radic Biol Med 2011; 51: 2060-2072.
[56] Gu Z, Li Y, Yang X, Yu M, Chen Z, Zhao C, Chen L and Wang L. Overexpression of CLC-3 is regulated by XRCC5 and is a poor prognostic biomarker for gastric cancer. J Hematol Oncol 2018; 11: 115.
[57] Wang J, Che W, Wang W, Su G, Zhen T and Jiang Z. CDKN3 promotes tumor progression and confers cisplatin resistance via RAD51 in esophageal cancer. Cancer Manag Res 2019; 11: 3253-3264.
[58] Fan C, Chen L, Huang Q, Shen T, Welsh EA, Teer JK, Cai J, Cress WD and Wu J. Overexpression of major CDKN3 transcripts is associated with poor survival in lung adenocarcinoma. Br J Cancer 2015; 113: 1735-1743.
[59] Song Q, He X, Xiong Y, Wang J, Zhang L, Leung EL and Li G. The functional landscape of Golgi membrane protein 1 (GOLM1) phosphoproteome reveal GOLM1 regulating P53 that promotes malignancy. Cell Death Discov 2021; 7: 42.
[60] Cox DJ, Strudwick N, Ali AA, Paton AW, Paton JC and Schroder M. Measuring signaling by the unfolded protein response. Methods Enzymol 2011; 491: 261-292.
[61] Zhao X, Yang Y, Yao F, Xiao B, Cheng Y, Feng C, Duan C, Zhang C, Liu Y, Li H, Xiao B and Dai R. Unfolded protein response promotes doxorubicin-induced nonsmall cell lung cancer cells apoptosis via the mTOR pathway inhibition. Cancer Biother Radiopharm 2016; 31: 347-351.
[62] Chanvorachote P, Sriratanasak N and Nonpanya N. C-myc contributes to malignancy of lung cancer: a potential anticancer drug target. Anticancer Res 2020; 40: 609-618.
[63] Waldman AD, Fritz JM and Lenardo MJ. A guide to cancer immunotherapy: from T cell basic science to clinical practice. Nat Rev Immunol 2020; 20: 651-668.
[64] Vanneman M and Dranoff G. Combining immunotherapy and targeted therapies in cancer treatment. Nat Rev Cancer 2012; 12: 237-251.
[65] Salamon P, Mekori YA and Shefler I. Lung cancer-derived extracellular vesicles: a possible mediator of mast cell activation in the tumor microenvironment. Cancer Immunol Immunother 2020; 69: 373-381.
[66] Bo X, Wang J, Suo T, Ni X, Liu H, Shen S, Li M, Wang Y, Liu H and Xu J. Tumor-infiltrating mast cells predict prognosis and gemcitabine-based adjuvant chemotherapeutic benefit in biliary tract cancer patients. BMC Cancer 2018; 18: 313.
[67] Stoyanov E, Uddin M, Mankuta D, Dubinett SM and Levi-Schaffer F. Mast cells and histamine enhance the proliferation of non-small cell lung cancer cells. Lung Cancer 2012; 75: 38-44.
[68] Virk H, Arthur G and Bradding P. Mast cells and their activation in lung disease. Transl Res 2016; 174: 60-76.

Table S2. The Kaplan-Meier estimator and univariate Cox model recognized potential prognostic genes (*p*-value < 0.05)

ID	KM_*p* value	HR	HR_95L	HR_95H	Cox_*p* value
A2M	0.03635591	0.865952386	0.767586037	0.976924407	0.019312523
AGFG1	0.005969821	1.557284476	1.187009783	2.043062302	0.001386026
AMT	0.000688087	0.706229679	0.584920058	0.852698334	0.000297883
BIRC5	0.000512744	1.225187869	1.087336185	1.380516288	0.000853495
BRCA1	0.003639305	1.294398812	1.051486381	1.593428422	0.014957799
CCNA2	7.60E-05	1.319065087	1.155949134	1.505198329	3.93E-05
CCNB1	0.000748649	1.33362251	1.163665557	1.528402202	3.49E-05
CD40LG	0.004450403	0.603035786	0.459661858	0.791129724	0.000260791
CDC45	0.009352153	1.225039592	1.06487204	1.409297968	0.004523127
CDK1	3.48E-05	1.273785278	1.116573093	1.453132756	0.00031753
CDKN3	0.000491463	1.317019834	1.150053539	1.508226517	6.85E-05
CTSH	0.014136377	0.797222352	0.709852616	0.895345688	0.000129958
CYB5A	0.017896263	0.847791437	0.733712337	0.979607789	0.025130929
CYCS	0.000678607	1.410693187	1.139902451	1.745811904	0.001555754
FBLN5	0.006211839	0.842754242	0.720859452	0.98526101	0.031853444
FKBP4	0.000656198	1.512177196	1.263554203	1.809720443	6.41E-06
GJB3	4.91E-05	1.286595672	1.172188403	1.412169256	1.14E-07
GMFB	0.044418626	1.382669098	1.060958477	1.801930874	0.016490709
GOLM1	0.004606133	1.283927731	1.092758192	1.508540893	0.002378666
GPR18	0.037110876	0.630993691	0.444531878	0.895668136	0.009980401
KIFC1	0.019722175	1.216917773	1.068563591	1.38586873	0.00307908
MGP	0.002194157	0.830807679	0.7420004	0.930243971	0.001310817
MS4A1	0.000646014	0.79028853	0.691254095	0.903511408	0.000570454
MTHFD2	0.007938215	1.217044681	1.037684728	1.427406337	0.015747404
PEBP1	0.000694846	0.603658936	0.464865289	0.78389185	0.000152746
PGPEP1	0.008388266	0.579023332	0.435016278	0.770702238	0.000180315
PIK3R1	0.001224051	0.740850366	0.578366037	0.948982528	0.017573195
PSEN1	0.042803167	1.574897514	1.035498553	2.39527344	0.033752401
PSTPIP1	0.001047455	0.745607296	0.589258229	0.943440775	0.014490901
RPS6KA1	0.004880836	0.590566723	0.443361394	0.786647325	0.000317583
SCNN1B	0.000434671	0.840445752	0.761426061	0.927665993	0.000559833
SELENBP1	0.024496317	0.836016789	0.753471769	0.927604856	0.000733344
SFTPB	0.000420472	0.909053377	0.868133865	0.95190163	4.96E-05
SFTPD	0.006936968	0.903031336	0.850333872	0.958994602	0.000884913
SLC2A1	4.18E-05	1.260694284	1.134365867	1.401091237	1.71E-05
SPHK1	0.034273147	1.324008324	1.132246235	1.548248066	0.000438349
ST3GAL4	0.009671338	1.239821144	1.052814974	1.460044269	0.009968083
STEAP1	4.88E-05	1.140063667	1.027349666	1.265143901	0.013588133
STXBP1	0.023049985	0.79530979	0.680537345	0.929438576	0.003974098
SYNE1	0.045716589	0.717043718	0.574109582	0.895563686	0.003363569
TK1	0.000278583	1.309411925	1.145019451	1.497406518	8.20E-05
TP73-AS1	0.033595176	0.672083258	0.510731802	0.884409202	0.004555332
UBE2C	0.036479194	1.160711037	1.05461661	1.277478562	0.002309194
VDAC2	0.007902772	1.592458648	1.213269074	2.090158398	0.000798918
XRCC5	0.011601889	1.801297672	1.281241219	2.5324453	0.000709821

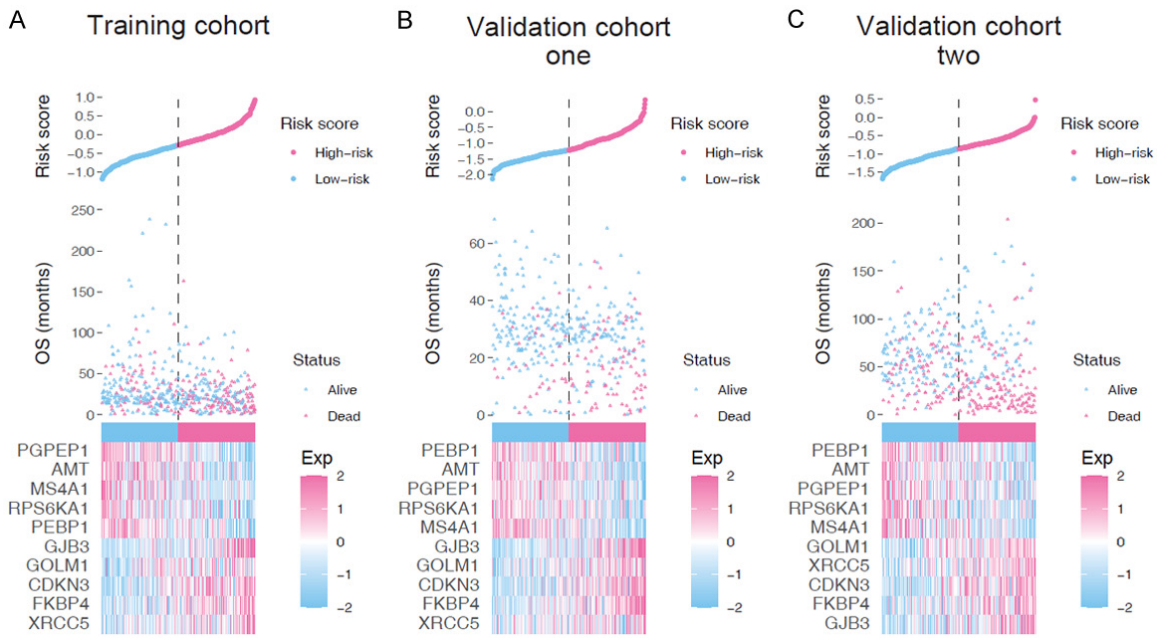

Figure S1. The distributions of the risk score, survival status, survival time, and ten genes' levels for LUAD cases in the training cohort (A), validation cohort one (B), and validation cohort two (C). All LUADs are listed in ascending order from left to right according to their risk scores (upper part), and their survival status and survival time are displayed in middle part. The hub genes relative expression of each patient is shown in the lower part. OS: overall survival; LUAD: lung adenocarcinoma.

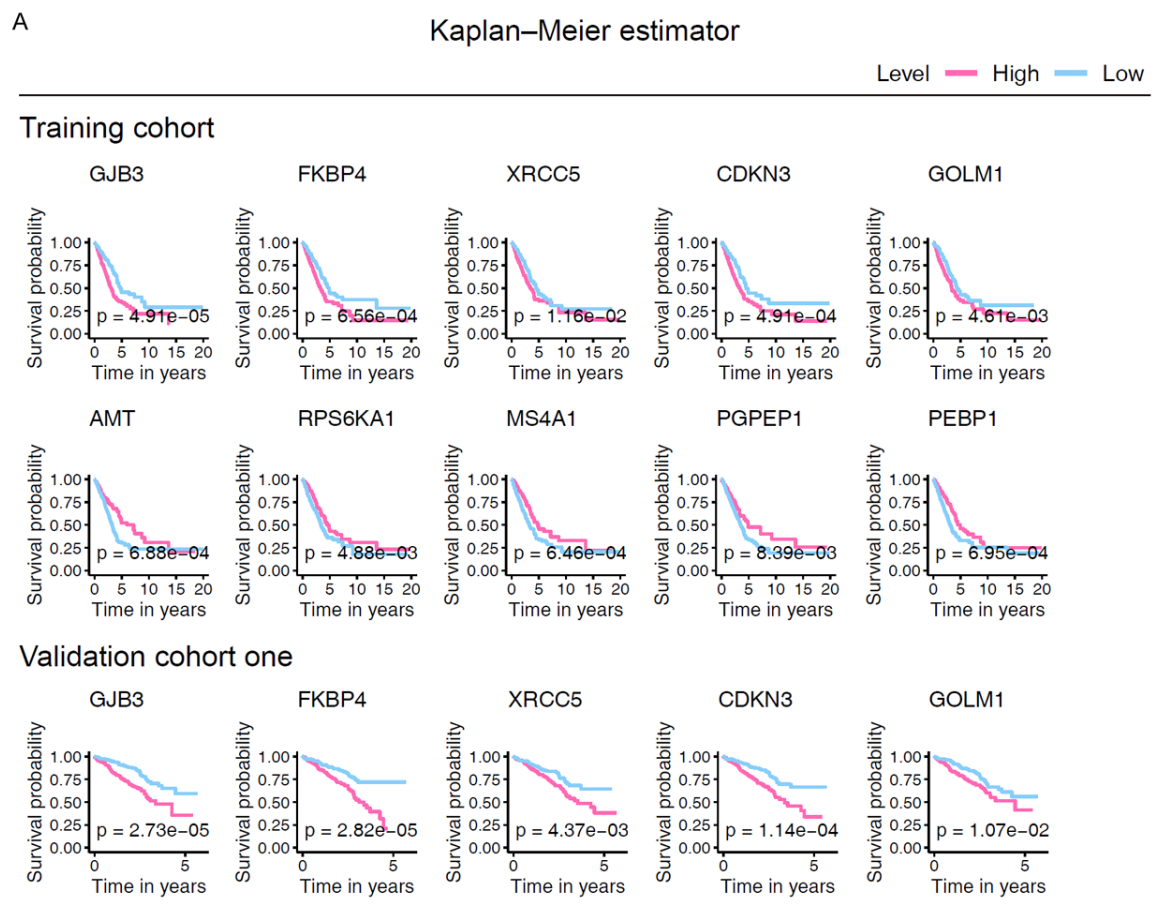

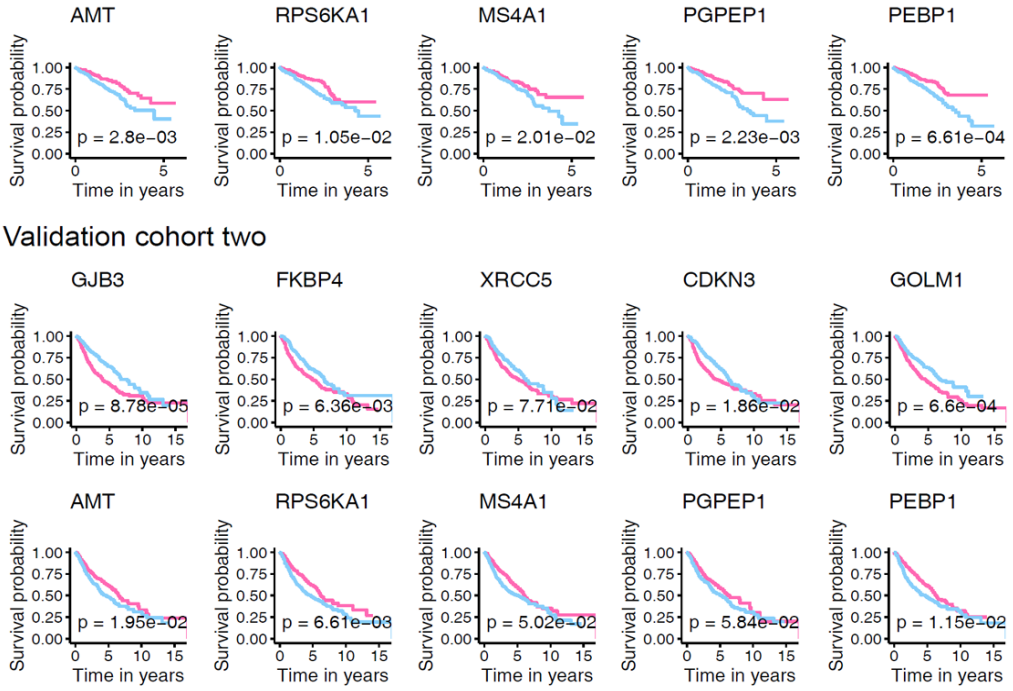

B

Univariate Cox regression

Variable	HR	Lower 95% CI	Upper 95% CI	P−value
Training cohort				
FKBP4	1.512	1.264	1.810	6.41e−06
AMT	0.706	0.585	0.853	2.98e−04
CDKN3	1.317	1.150	1.508	6.85e−05
XRCC5	1.801	1.281	2.532	7.10e−04
GOLM1	1.284	1.093	1.509	2.38e−03
PEBP1	0.604	0.465	0.784	1.53e−04
MS4A1	0.790	0.691	0.904	5.70e−04
RPS6KA1	0.591	0.443	0.787	3.18e−04
GJB3	1.287	1.172	1.412	1.14e−07
PGPEP1	0.579	0.435	0.771	1.80e−04
Validation cohort one				
FKBP4	2.047	1.500	2.794	6.39e−06
AMT	0.518	0.387	0.692	8.38e−06
CDKN3	1.316	1.132	1.530	3.61e−04
XRCC5	3.825	1.527	9.577	4.18e−03
GOLM1	1.721	1.286	2.304	2.64e−04
PEBP1	0.252	0.134	0.473	1.80e−05
MS4A1	0.876	0.798	0.961	5.06e−03
RPS6KA1	0.536	0.384	0.748	2.44e−04
GJB3	1.376	1.223	1.549	1.19e−07
PGPEP1	0.597	0.406	0.879	8.91e−03
Validation cohort two				
FKBP4	1.266	1.022	1.567	3.06e−02
AMT	0.791	0.644	0.971	2.51e−02
CDKN3	1.236	1.057	1.445	7.96e−03
XRCC5	1.517	1.143	2.014	3.96e−03
GOLM1	1.193	1.044	1.364	9.80e−03
PEBP1	0.758	0.602	0.954	1.83e−02
MS4A1	0.894	0.809	0.987	2.70e−02
RPS6KA1	0.628	0.482	0.817	5.34e−04
GJB3	1.227	1.111	1.354	5.07e−05
PGPEP1	0.734	0.540	0.997	4.75e−02

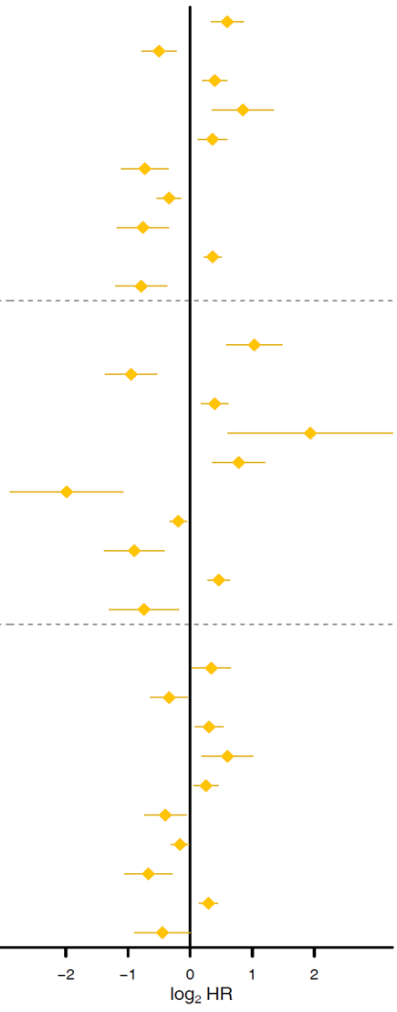

Figure S2. The Kaplan-Meier analysis (A) and univariate Cox models (B) established in the studied cohorts testing the predictive ability of each hub gene. Patients were grouped based on their median risk score. The Kaplan-Meier method compared the survival difference between high and low-risk patients, and the log-rank test examined the significance. HR: hazard ratio; *P*-value < 0.05 is considered as significantly.

Table S3. The significant pathways that were detected in the GSEA analysis (p<0.05 and FDR<0.25)

Term	ES	NES	p	FDR	FWER
UNFOLDED_PROTEIN_RESPONSE	0.5884	2.3847	0	0	0
GLYCOLYSIS	0.61	2.4193	0	0	0
MYC_TARGETS_V1	0.7787	2.5074	0	0	0
MTORC1_SIGNALING	0.7022	2.5633	0	0	0
MYC_TARGETS_V2	0.7924	2.257	0	0.0005	0.003
G2M_CHECKPOINT	0.8341	2.201	0	0.0012	0.006
E2F_TARGETS	0.8562	2.0977	0	0.0043	0.021
DNA_REPAIR	0.4932	2.0467	0	0.0054	0.033
PROTEIN_SECRETION	0.507	2.0514	0.0073	0.006	0.032
MITOTIC_SPINDLE	0.6305	1.9618	0.002	0.0115	0.066
HYPOXIA	0.5011	1.8854	0.006	0.0179	0.096
UV_RESPONSE_UP	0.3971	1.8279	0.002	0.0245	0.135
ANDROGEN_RESPONSE	0.4641	1.7816	0.0216	0.0325	0.182
ESTROGEN_RESPONSE_LATE	0.4224	1.7404	0.0082	0.0407	0.223
SPERMATOGENESIS	0.4702	1.6864	0.0142	0.0536	0.294
PI3K_AKT_MTOR_SIGNALING	0.3777	1.6359	0.0393	0.069	0.366
CHOLESTEROL_HOMEOSTASIS	0.4304	1.5691	0.033	0.0958	0.469

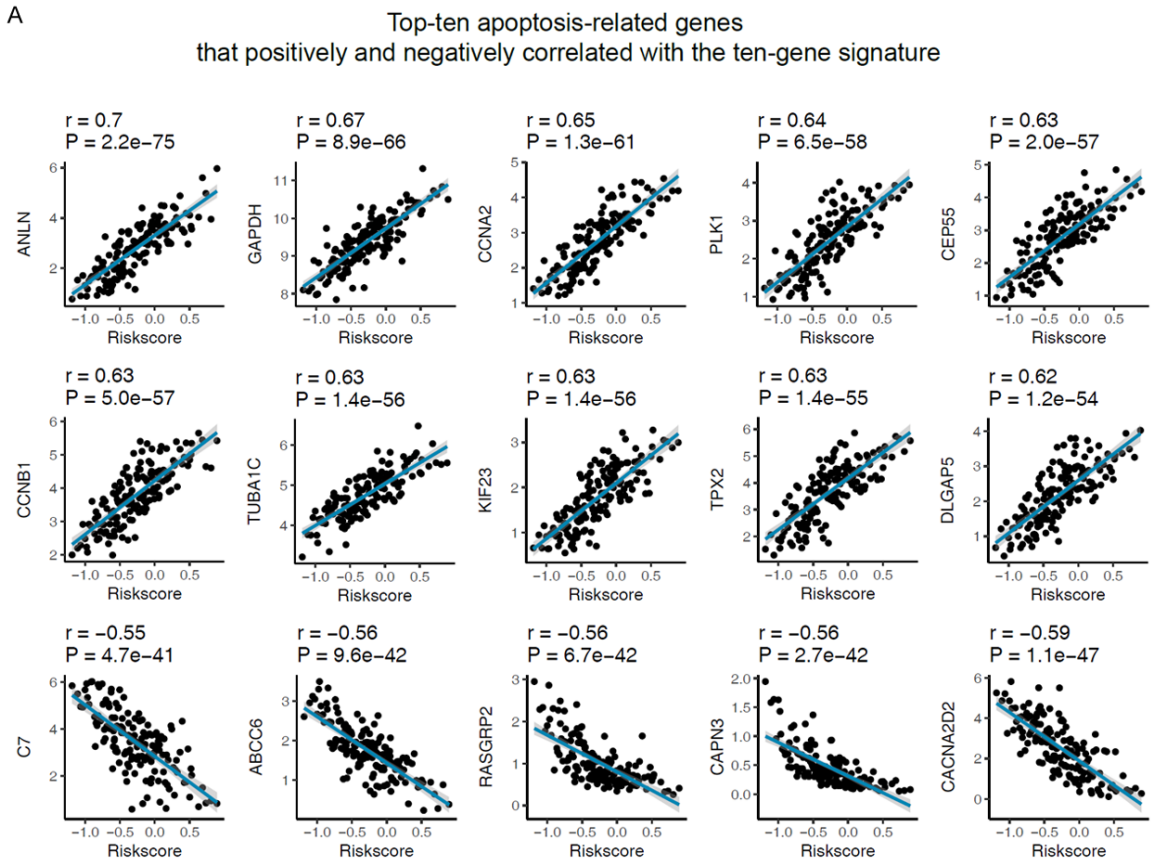

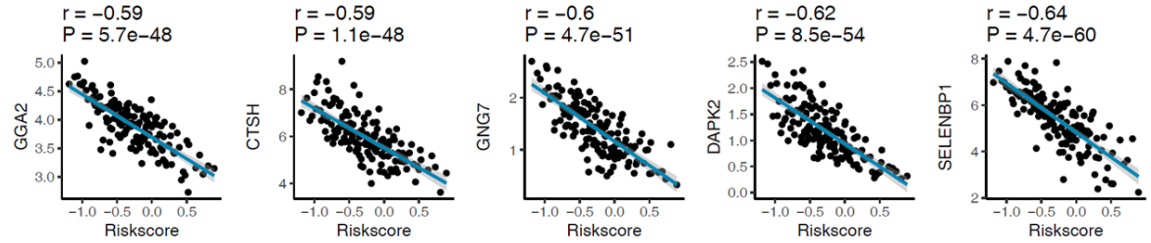

B

Top necroptosis-related genes
that positively and negatively correlated with the ten-gene signature

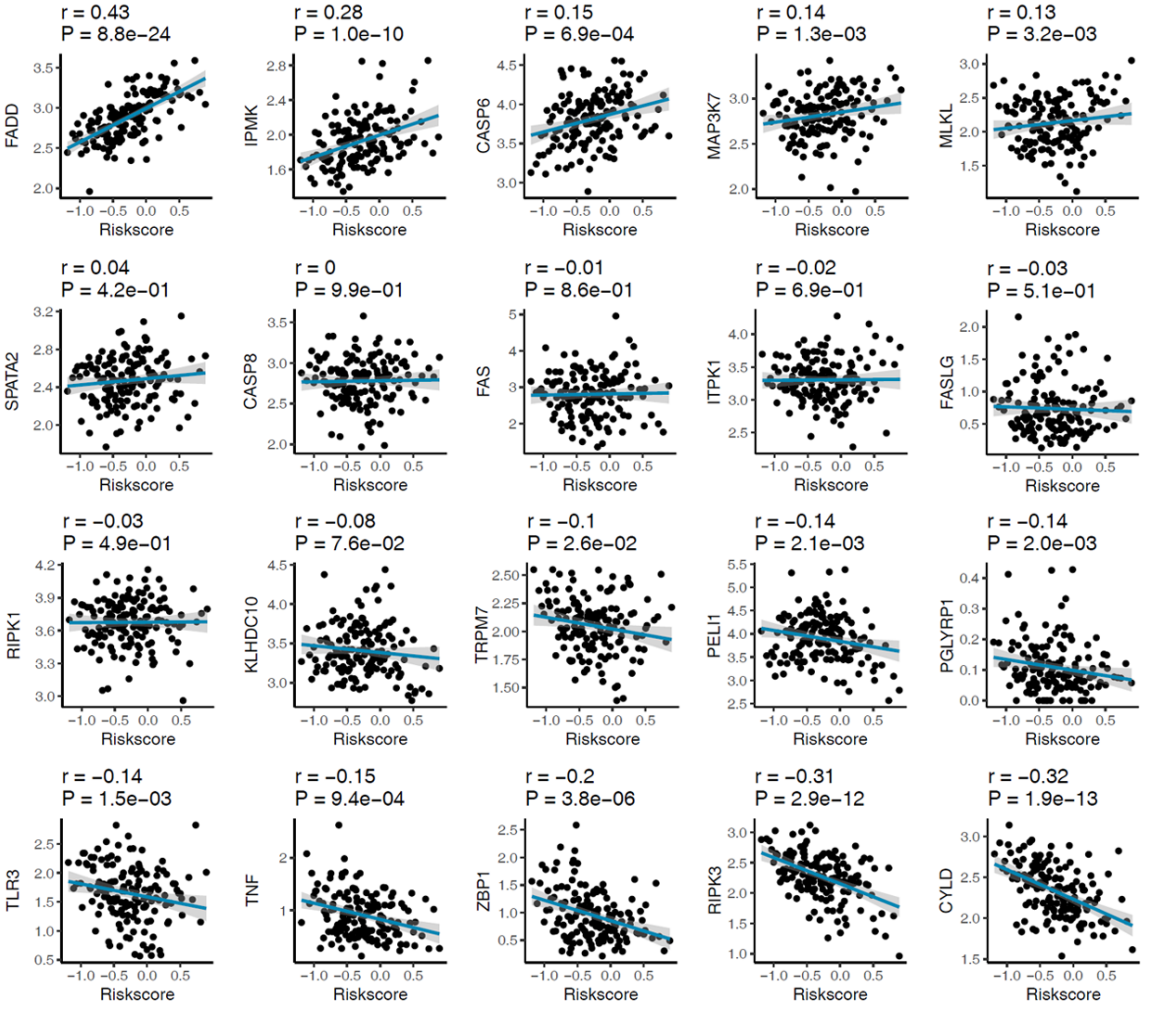

C

Top-ten pyroptosis-related genes
that positively and negatively correlated with the ten-gene signature

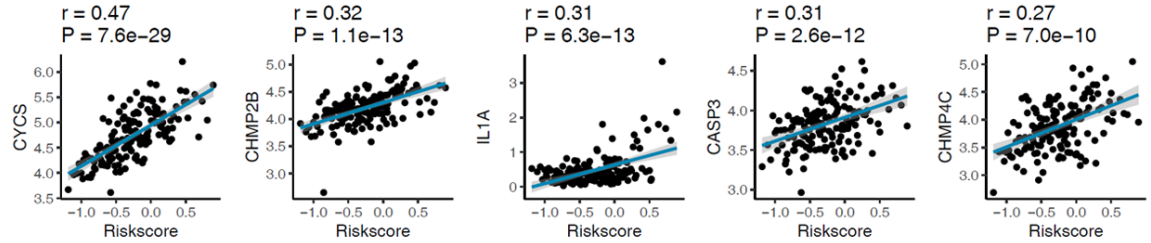

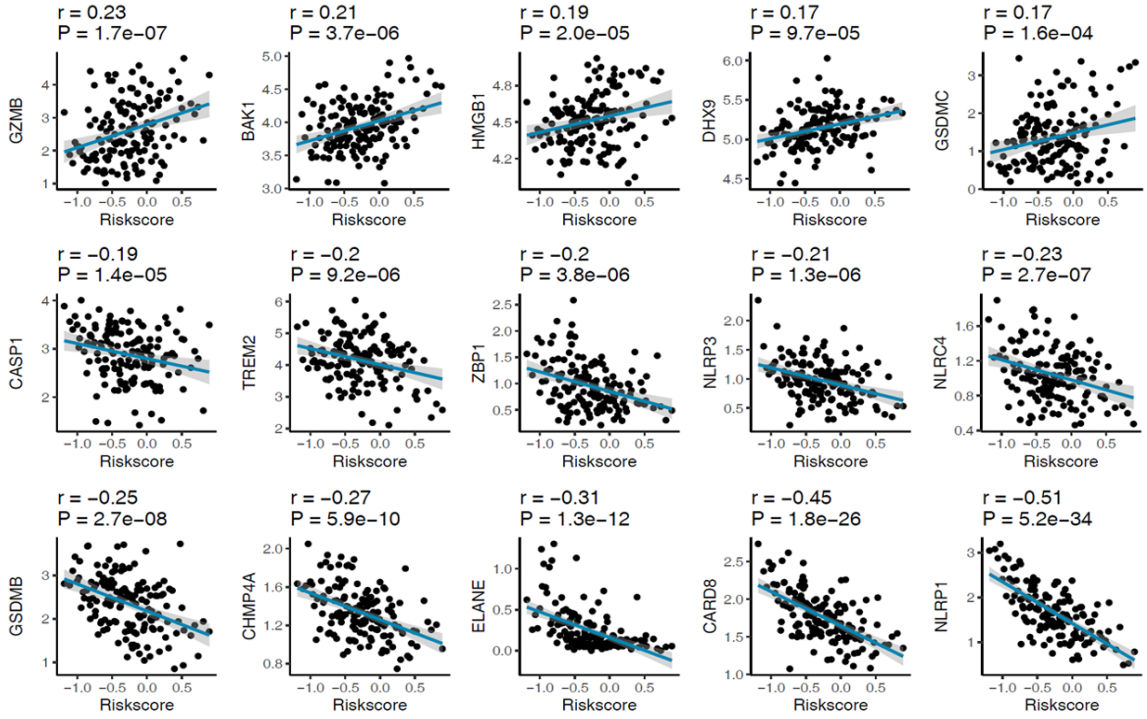

D

Top-ten ferroptosis-related genes
that positively and negatively correlated with the ten-gene signature

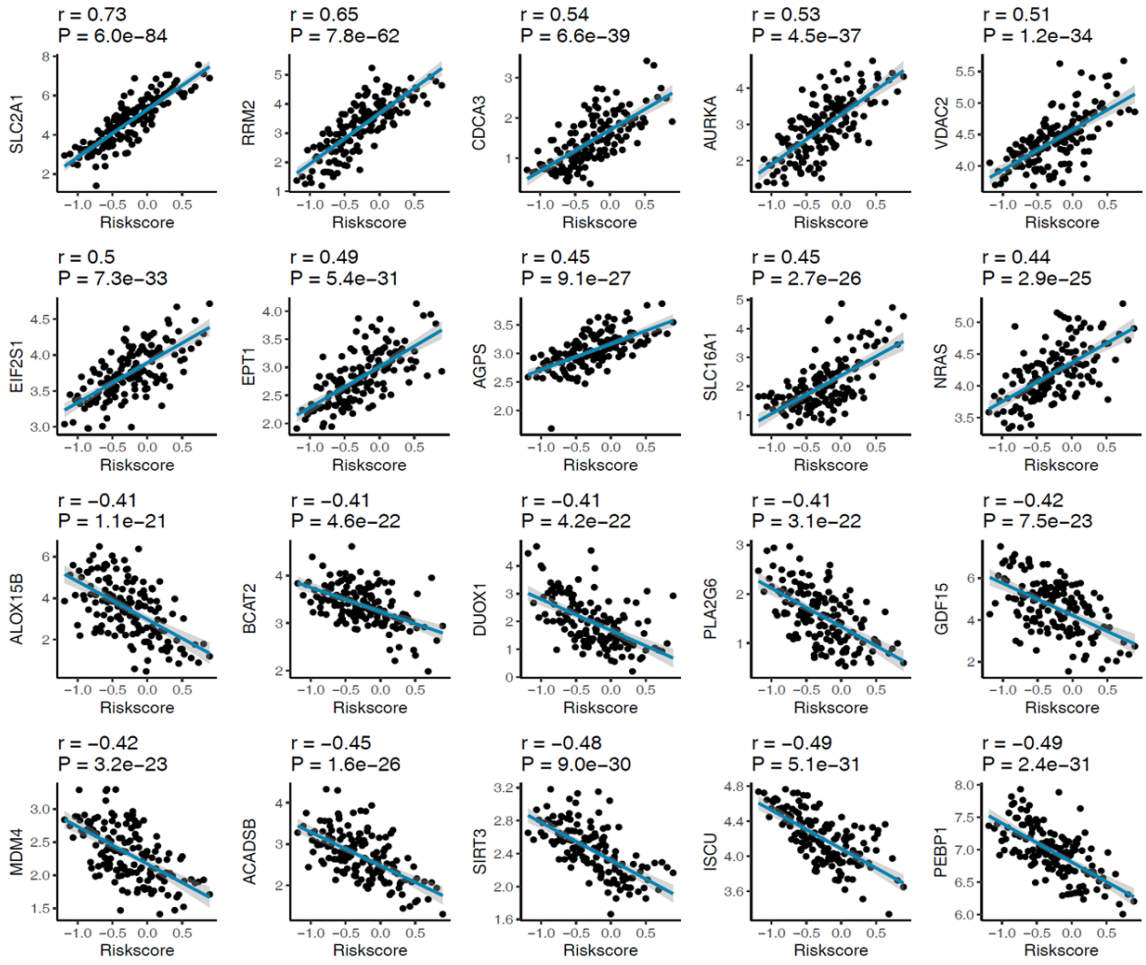

Figure S3. The correlations between the ten-gene signature and apoptosis (A), necroptosis (B), pyroptosis (C), and ferroptosis (D) related genes in the training cohort. Only top correlations were plotted. The Pearson examination was carried out for correlation test.

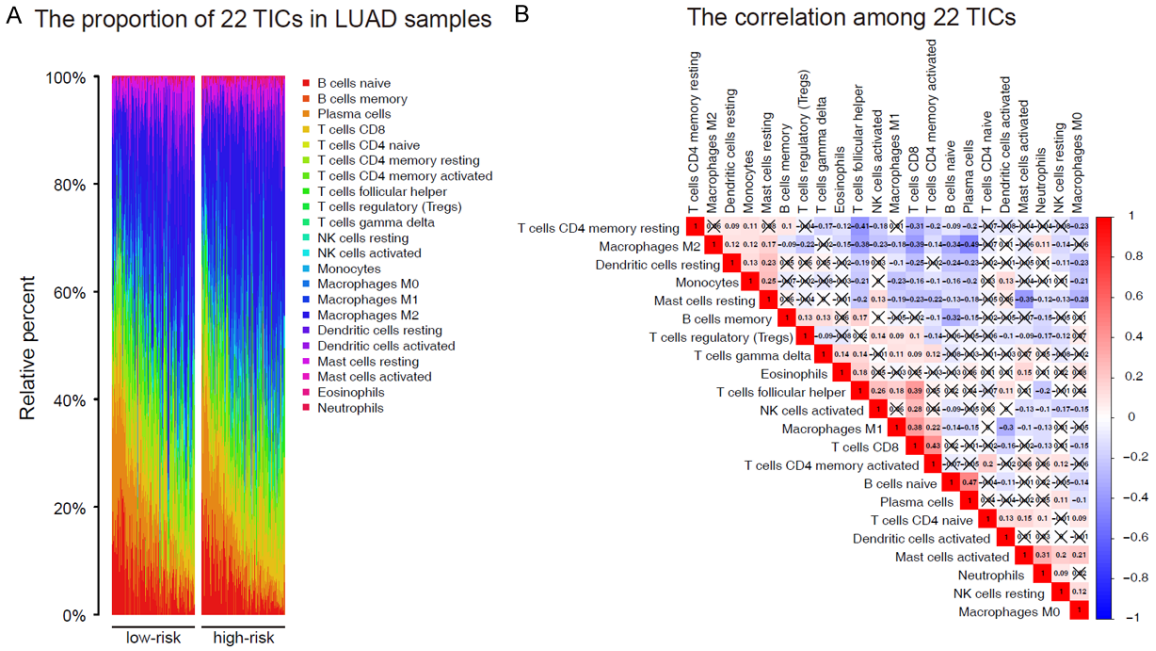

Figure S4. Identification of 22 TICs distribution and their mutual internal relationships in LUADs. LUAD patients were grouped according to the median risk score. A. We displayed the distributions of 22 TICs in high and low-risk LUADs in bar graph. B. Correlation among 22 TICs detected by Pearson coefficient. *P*-value < 0.05 is considered significant. TIC: tumor-infiltrating immune cell; LUAD: lung adenocarcinoma.

Table S5. Correlations of risk score with 22 kinds of TICs tested by Pearson coefficient

TIC	r	*p*-value
Mast cells resting	-0.317643279	3.49E-13
T cells CD4 memory resting	-0.231546267	1.64E-07
B cells memory	-0.223983323	4.19E-07
Monocytes	-0.173246186	9.87E-05
T cells regulatory (Tregs)	-0.134370068	0.002606029
Plasma cells	-0.116668829	0.009022841
Dendritic cells resting	-0.103880197	0.020162682
B cells naive	-0.093952242	0.035709027
Eosinophils	0.00375334	0.933281073
NK cells resting	0.058399276	0.192338627
NK cells activated	0.060118331	0.179551798
Macrophages M2	0.069367219	0.121361923
T cells follicular helper	0.084551609	0.058853829
T cells gamma delta	0.086093431	0.054371805
T cells CD4 naive	0.128221154	0.004081428
Dendritic cells activated	0.145338326	0.001117858
Macrophages M1	0.169104063	0.000145156
Mast cells activated	0.181257916	4.57E-05
T cells CD8	0.186636691	2.67E-05
Macrophages M0	0.219748632	6.97E-07
Neutrophils	0.259109739	4.10E-09
T cells CD4 memory activated	0.2793269	2.05E-10

Table S6. Prognostic capacity of 22 TICs examined by Kaplan-Meier analysis

TIC	*p*-value
B cells naive	0.731955731
B cells memory	0.145264777
Plasma cells	0.07168164
T cells CD8	0.949457769
T cells CD4 naive	0.151571969
T cells CD4 memory resting	0.983427527
T cells CD4 memory activated	0.063337318
T cells follicular helper	0.612899091
T cells regulatory (Tregs)	0.570358661
T cells gamma delta	0.877261838
NK cells resting	0.420059349
NK cells activated	0.650309228
Monocytes	0.347772347
Macrophages M0	0.157737947
Macrophages M1	0.073909277
Macrophages M2	0.251093491
Dendritic cells resting	0.044346026
Dendritic cells activated	0.671178187
Mast cells resting	0.000163805
Mast cells activated	0.008103067
Eosinophils	0.602112244
Neutrophils	0.922155496